LADON, a natural antisense transcript of *NODAL*, promotes metastasis in melanoma by repressing *NDRG1*

Dutriaux Annie[1], Diazzi Serena[1], Caburet Sandrine[2], Bresesti Chiara[1], Hardouin Sylvie[1], Deshayes Frédérique[3], Collignon Jérôme[1,*] and Flagiello Domenico[1*]

1: Université de Paris, CNRS, Institut Jacques Monod, Regulation of Cell-Fate Specification team, Paris 75013, France

2: Université de Paris, CNRS, Institut Jacques Monod, Molecular Oncology and Ovarian Pathologies team, Paris 75013, France

3: Université de Paris, CNRS, Institut Jacques Monod, Morphogenesis, Homeostasis and Pathologies team, Paris 75013, France

*Correspondence: jerome.collignon@ijm.fr; domenico.flagiello@ijm.fr

Summary

The TGFβ family member NODAL, primarily known for its role during embryonic development, has also been associated with tumor progression in a number of cancers. Some of the evidence supporting its involvement in melanoma has appeared contradictory, suggesting that NODAL in this context might rely on a non-canonical mode of signaling. To investigate this possibility we studied how a deletion of *NODAL* affected cell behavior in a metastatic melanoma cell line. The mutation does prevent melanoma cells from acquiring an invasive behavior. However, this phenotype was found to result not from the absence of NODAL, but from the disabled expression of a natural antisense transcript of *NODAL* now called *LADON*. Its expression promotes the mesenchymal to amoeboid transition that is critical to melanoma cells' invasiveness. Our analyses revealed that the increase in *LADON* expression necessary to complete this transition is dependent on WNT/β-CATENIN signaling and that its downstream effectors include MYCN and the metastasis suppressor NDRG1, which controls changes in the cytoskeleton. These results identify *LADON* as a player in the network of interactions governing tumor progression in melanoma, and suggest a similar implication in other cancer types.

Keywords: lncRNA, metastasis, melanoma, A375, CRISPR/Cas9, β-CATENIN, pMLC2, amoeboid.

Introduction

Metastasis is responsible for up to 90% of cancer deaths (Chaffer and Weinberg 2011), making the determination of the molecular components involved in invasion and metastasis crucial to the improvement of diagnosis and treatment. The *NODAL* gene, which encodes a TGFβ family member, has been presented as a possible candidate (Quail et al. 2013; Topczewska et al. 2006). It is best known for its role during development, where it is required both to maintain the undifferentiated state of embryonic precursors and to specify the identity of specific cell types, including several motile cell types (Robertson 2014). It is also expressed in the adult, notably in tissues that undergo periodical renewal or remodeling under the control of hormonal stimuli, such as the endometrium and the mammary gland (Bianco et al. 2002; Papageorgiou et al. 2009). Its expression in tumor cells has been correlated with the plasticity and invasive behavior of these cells (Bodenstine et al. 2016; Quail et al. 2013), a credible echo of its functions in embryonic and adult tissues.

The involvement of *NODAL* in tumor progression and metastasis was first described in melanoma cell lines, where inhibition of NODAL signaling was found to reduce invasiveness, colony formation and tumorigenicity, and to promote reversion toward a melanocytic phenotype (Topczewska et al., 2006). The impact of NODAL signaling in melanoma was associated with the failure of melanoma cells to express LEFTY (Postovit et al., 2008; Costa et al., 2009), a known antagonist of NODAL, which in the embryo is usually dependent on NODAL signaling for its expression. Also, the expression of CRIPTO, an obligatory co-receptor of NODAL, was found to be weak in metastatic melanoma cell lines, and restricted to a small cell subpopulation (Postovit et al., 2008). Furthermore, the size of the protein identified as the NODAL precursor in these studies appeared smaller than that of the NODAL precursor previously characterized (Constam & Robertson, 1999; Le Good et al., 2005). Intriguingly, semi-quantitative PCR analyses suggested that the most abundant *NODAL* transcripts in an aggressive melanoma cell line did not include the third exon of the gene (Strizzi et al., 2012), which encodes an essential part of the mature ligand. Many of the findings related to the expression and role of *NODAL* in melanoma therefore appear contradictory and difficult to reconcile with its reliance on canonical SMAD2,3-dependent NODAL signaling. There are a few situations in vertebrate embryos where *NODAL* has been found to act independently of SMAD2,3, involving for example the binding of its uncleaved precursor to an FGF receptor complex or a ligand-independent function of its mRNA (Ellis et al., 2015; Lim et al., 2012). Melanoma thus might be a case where a non-canonical mode of action of *NODAL* is involved, in particular one of those already found in other contexts or another one as yet undescribed,.

To investigate the mechanism underlying the implication of *NODAL* in melanoma we used genome editing to create a loss-of-function mutation of the gene in the metastatic melanoma cell line A375, a recognized cell culture model for this type of cancer, previously

reported as *NODAL*-expressing (Topczewska et al. 2006). The mutation drastically reduced the capacity of these cells to acquire an invasive phenotype. However, the exogenous inhibition or stimulation of ACTIVIN/NODAL signaling had no effect on the behavior of A375 cells, and we could not detect actual *NODAL* expression in these cells, implying that neither the NODAL ligand nor *NODAL* mRNAs played a part in this phenotype. We found instead that the mutation disabled the expression of a natural antisense transcript, now called *LADON*, which overlaps with *NODAL* exon2 and has thus far largely gone unnoticed. Our investigations of its role in the A375 cell line show that it is responding to signals known to control tumor progression and metastasis, and that it regulates the expression of known oncogenes and tumor suppressors. This study thus identifies *LADON* as a novel regulator of the metastatic process.

Results

The invasive behavior of A375 cells is dependent on the presence of *NODAL* exon2

We used RT-PCR analysis to characterize *NODAL* expression in a small panel of cell lines. A primer pair restricted to *NODAL* exon2 detected a band in all of them (Fig. S1A). In contrast, a primer pair spanning exon2 and 3 (Figure 1A) detected no transcript in metastatic melanoma cell lines (A375, 888, SLM) (Figure S1B), while a band of the expected size was present in a fetal kidney cell line (HEK293). These results are consistent with the presence of exon2-containing transcripts described in other melanoma cell lines (Strizzi et al., 2012). They are also consistent with the lack of full-length *NODAL* transcripts reported more recently in another panel of melanoma cell lines (Donovan et al., 2017). To test for a possible requirement for *NODAL* exon2 during key steps of the metastatic process we used genome editing to delete it in A375 cells (Figure 1A). Five of the independent mutant clones thus obtained, designated A375ΔE2a to e, were selected for further characterization (Figures S1C and S1D). We found that the absence of *NODAL* exon2 impaired their ability to close the gap in a 2D wound-healing (scratch) assay (Figure 1B and 1C), suggesting that their motility and/or their proliferation had been drastically reduced. However, treating A375 cells with increasing concentrations of recombinant ACTIVIN or NODAL, which can both activate the same SMAD2,3-dependent signaling pathway, had no effect on their behavior in the same assay (not shown). Treatment with SB431542, a pharmacological inhibitor of the ACTIVIN/NODAL type I receptors ALK4, 5 and 7, had no effect either (not shown).

The impact of the deletion on the behavior of A375 cells implies that these cells require *NODAL* exon2 to adopt their invasive phenotype, but their lack of response to the ligands and to the inhibition of the ACTIVIN/NODAL signaling pathway, together with the absence of full-length *NODAL* transcripts, suggests that the gene's mode of action does not involve its regular signaling function.

***A* natural antisense transcript overlaps with *NODAL* exon2 in melanoma cell lines**

Consultation of the *Ensembl* database revealed an updated version of the human *NODAL* locus, featuring a novel transcript in addition to the 2 *NODAL* splice variants already known (Figure 1A and 1D). This 1728nt long transcript (AC022532) is transcribed from the plus strand (opposite to *NODAL*). The corresponding cDNA was originally characterized as being full-length (Ota et al., 2004), a claim consistent with the subsequent identification of similar homolog transcripts in Chimpanzee and in Orangutan, respectively 1742 and 1746nt long (Ensembl database). Interestingly, a similar transcript is not found in mouse, rat and other vertebrate models. In human it starts 450bp upstream and ends 560bp downstream of *NODAL* exon2, and therefore includes a sequence complementary to that of the entire exon. This natural antisense transcript (NAT) contains an ORF, but since no corresponding protein has been reported so far (a likely consequence of the absence of a proper Kozak consensus sequence at the ATG), it is identified as non-coding. To confirm that this antisense transcript was present in A375 cells we reverse-transcribed total A375 RNA using either reverse (N2F) or forward (N2R) primers with respect to the expected orientation of its transcription. The resulting cDNAs were used to PCR-amplify sequences spanning exon2 and the adjoining 5' or 3' regions (Figure 1A). The fact that a band of the expected size was only obtained with cDNAs transcribed using the reverse primer N2F demonstrated the presence of the antisense transcript (Figure S1E). The corresponding transcription unit is designated as *LADON* hereafter.

We used a specific pair of primers (Figure 1A) to detect *LADON* transcripts in the same panel of cancer cell lines as before, and amplified a band of the expected size in all of them (Figure S1F). RT-PCR analysis of *LADON* expression in the melanocyte and melanoma cell lines of our panel detected a 2- to 3-fold increase between 24h and 96h of culture in metastatic but not in non-metastatic cell lines (Figure 1E). In contrast, A375ΔE2 clones expressed a truncated *LADON* transcript (*LADON-ΔE2*), reduced to the 5' and 3' parts that flank exon2 (Figure 1A and S1G), and this expression showed no sign of increase after 96h in culture, implying that the deletion deprived *LADON* of a critical regulatory input (Figure 1F). In an echo of earlier claims linking *NODAL* expression and melanoma progression (Topczewska et al., 2006), these results suggest that the capacity of melanoma cell lines to increase *LADON* expression correlates with their capacity to metastasize.

To assess the expression of *LADON* in other cell types and cancer cell lines we analyzed strand-specific RNA-seq data produced by the ENCODE project. This analysis found that *LADON* is expressed in many cell types and cancer cell lines, while *NODAL* is expressed far less frequently (Figures 1D and S2A). It confirmed notably the absence of *NODAL* expression in melanocytes and melanoma cell lines (Figure 1D). *NODAL* expression was detected in a

few cell lines, such as keratinocytes or breast cancer lines, but except in human embryonic stem cells its level was always rather low (Figures 1D and S2A).

We noticed that in a number of *LADON*-expressing cell lines, the corresponding reads extended further upstream on the plus strand, possibly up to the adjacent gene, *EIF4EBP2*, which is transcribed from the same strand as *LADON*. This suggested that the transcription of *LADON* could be initiated upstream of the position currently indicated by the data compiled in *Ensembl* (Figures 1D and S2A). To assess this possibility we performed PCR on cDNAs reverse-transcribed, using again the *LADON*-binding primer N2F (Figure S1H). The PCR bands obtained with primer pairs positioned between *EIF4EBP2* and *LADON* revealed that some *EIF4EBP2* transcripts extend further in 3' and include sequences that we have identified as being part of *LADON* (Figure S1H and S1I). However, RT-qPCR showed that it is a transcript starting within the last *NODAL* intron that is accounting for the majority of *LADON* expression in A375 cells cultured for 3 days (Figure S1J).

These results confirmed that the absence of *NODAL* did not cause the changes in behavior we characterized in cells deleted for *NODAL* exon2. They led us to identify *LADON* as a candidate for this cellular phenotype, and to investigate the link between the shared propensity of metastatic cell lines to give rise to metastatic cells and their capacity to upregulate *LADON*.

A375 cells secrete factors that promote *LADON* expression and cell motility

To investigate what controlled the increase in *LADON* expression in the A375 cell line, we first tested its dependence on cell density (Kim et al. 2017). *LADON* transcript levels measured after 24h culture in cells seeded at high (80%) density were actually no different from those measured in cells seeded at low (20%) density (Figure 2A). The increase in *LADON* expression found after 72h culture in cells seeded at low density was therefore likely to depend on the duration of the culture but not on cell density. We investigated the possibility that the expression of *LADON* is dependent on secreted factors accumulating in the culture medium as follows. A375 cells were grown in standard medium (SM) with or without 10% FCS (to control for the possible effect of nutrient depletion), and three days later, when the cells reached high density, the media were collected. These A375-conditioned media (CM) were used to culture cells seeded at low density for 24h. For A375 cells these treatments resulted in a 2.4-fold increase in the expression of *LADON* (Figure 2B), compared to its expression level when cultured in SM. In contrast, the same treatments had no effect on *LADON* expression in the non-tumorigenic non-metastatic MNT1 cell line (Figure 2C). Interestingly, we found that medium conditioned by MNT1 cells could also trigger an increase in *LADON* expression in A375 cells (Figure 2C) while it elicited no such response in MNT1 cells themselves (Figure 2B). These results show that while both A375 and MNT1 cells

secrete and accumulate *LADON*-inducing factors in their culture media, only A375 cells are able to respond accordingly. This suggests that the ability to respond to *LADON*-inducing factors is a trait that distinguishes metastatic from non-metastatic cell lines.

We analyzed the published content of A375 cell-derived exosomes (Xiao et al., 2012), and detected a relative enrichment in *LADON* transcripts (Figure S2B). This raised the question of their possible contribution to the inductive capacity of the CM. We therefore analyzed the effect on A375 cells of a CM obtained from A375ΔE2 cells (A375ΔE2-CM). We found that this *LADON*-depleted CM had the same capacity to induce *LADON* expression as that obtained from A375 cells (Figure 2D), implying that *LADON* is not required in the CM to increase its own expression. Cells from A375ΔE2 clones, however, failed to increase the expression of the *LADON-ΔE2* transcript when exposed to the same CM (Figure 2E), confirming that the capacity of the locus to respond to these treatments is dependent on the presence of exon2 in the responding cells.

We noticed a difference in cell morphology in the cultures exposed to CM, reminiscent of changes described in migrating melanoma cells. Such cells rely on two inter-convertible modes of migration, designated mesenchymal and amoeboid (Friedl and Wolf 2010; Sanz-Moreno et al. 2008), with the faster amoeboid mode being the most efficient to drive tumor metastasis (Gadea et al. 2007; Paňková et al. 2010; Sanz-Moreno et al. 2011). We therefore investigated the effect of the A375-CM on cell morphology and migratory behavior. The mesenchymal to amoeboid transition (MAT), which involves a change from an elongated to a smaller and rounded cell morphology, was monitored via F-actin staining (Figure 2F) (Sahai and Marshall 2003). In SM no clear difference was seen between cultures of mutant and unmodified A375 cell populations, both showing similar percentages of elongated (25%) and rounded (75%) cells (not shown). However, when grown in CM, A375 cells saw an increase of the rounded cell fraction from 75% to 98% (Figure 2F). When the capacity of these cells to transmigrate through a collagen layer was quantified over a 24h period, this change in the composition of the population was associated with a 5-fold increase in the rate of transmigration (Figure 2G). In contrast, A375ΔE2 cells, which in SM had a transmigration rate a tenth of that of A375 cells, saw no improvement in their transmigration ability when cultured in CM (Figure 2H). *LADON* is therefore endowing A375 cells with the capacity to undergo CM-induced changes in cell behavior. Again, to assess the contribution of *LADON* itself to this particular effect of the CM we analyzed the effect of the A375ΔE2-CM on A375 cells. We found that while treated cells showed significant increases in the fraction of rounded cells (Figure 2F) and in their transmigration rate (Figure 2G), these changes were not as important as those obtained with the CM from A375 cells, implying that the inducing capacity of the CM relies on both *LADON*-dependent and *LADON*-independent components.

To confirm that it is the depletion of the *LADON* transcript and not another unrelated consequence of the deletion that is causing invasiveness to drop, we examined how

knocking-down LADON expression affects the behavior of A375 cells. Three different siRNAs located at the 5' end of the gene were tested. RT-PCR results showed a significant decrease of *LADON* expression with two of them, used alone or together (Figure S2C). The knockdown (KD) of *LADON* severely impaired the ability of A375 cells to transmigrate through a collagen monolayer over 24h, a behavior reminiscent of that of A375ΔE2 clones (Figure 2I). Interestingly, we also noticed that *LADON* KD cells systematically reached confluence earlier than controls (Figure S2D), suggesting that their proliferation rate was positively impacted, an observation consistent with these cells maintaining a non-invasive behavior (Carreira et al., 2006; Hoek et al., 2008).

Taken together, these results show that the expression of *LADON* in melanoma cells conditions both their capacity to produce factors that promote changes in cell behavior conducive to metastasis (i.e., MAT, increase in motility, decrease in proliferation), and their capacity to respond to such factors.

LADON expression is dependent on WNT/β-CATENIN signaling.

The MAT has been associated with increased stemness and clonogenic features of cancer cells (Taddei et al. 2014). To identify pathways possibly involved in the regulation of *LADON* expression, we used an RT2 profiler array (Qiagen) designed to track the expression levels of 84 genes relevant to the stemness of human cancer cells. The analysis was performed on mRNAs extracted from A375 cells cultured for 24h and 96h. The comparison of the profiles thus obtained revealed both up-regulated and down-regulated genes. The most important changes in expression were the up-regulation of *MYCN*, a proto-oncogene, and the down-regulation of *DKK1*, which encodes a component of the WNT/β-CATENIN signaling pathway (Figure 3A; Figure S3B). As genes for other components of this pathway (*WNT1*, *FZD7*) were also showing important variations (Figure 3A, S3B,C), and as *MYCN* is known to promote its activation in breast cancer cells (Ma et al. 2010), we tested its implication. A western blot (WB) analysis of β-CATENIN at regular time points over a 96h culture revealed an increase of the active, unphosphorylated, form of β-CATENIN within 48h, whereas total β-CATENIN levels remained unchanged (Figure 3B). This was associated with a continuous and steady increase in *LADON* expression over the entire length of the culture (Figure 3C). It was also confirmed that treatment with A375-CM for 24h increases β-CATENIN activation (Figure 3B). Next, we added recombinant WNT3A to cultured A375 cells. WB analysis showed that 24h treatment with increasing concentrations of WNT3A first led to increases in the active form of β-CATENIN but reached a plateau at 60ng/ml, while total β-CATENIN levels were unaffected (Figure 3D). To confirm that this resulted in a higher activity of the pathway, we quantified the expression levels of *AXIN2* - a known target of β-CATENIN (Jho et al. 2002) -

after the same treatments, and found that they increased in a dose-dependent manner (Figure 3E). The same treatments elicited a similar response from *LADON* for WNT3A concentrations above 30 ng/ml (Figure 3F), suggesting that this increase might be dependent on WNT/β-CATENIN signaling. To confirm this, we used the pharmacological inhibitor IWR-1-endo, which stabilizes the β-CATENIN destruction complex member AXIN2. After 48h of treatment we observed, as expected, a decrease in the level of the active β-CATENIN (Figure 3G), and a concomitant and identical decrease in the expression levels of *AXIN2* and *LADON* (Figure 3H).

A previous study conducted in the A375 cell line having established that the mitogen-activated protein kinase (MAPK) signaling pathway inhibits WNT/β-CATENIN signaling (Biechele et al. 2012), we also investigated the impact of a 24h treatment with the MAPK inhibitor PD98059 on *LADON* expression. WB analysis showed that the elimination of the active, phosphorylated, forms of extracellular signal-regulated kinase (ERK) 1 and 2 (Figure 3I) leads to a dramatic decrease of the active, phosphorylated, forms of glycogen synthase kinase-3 (GSK3) α and β. This resulted in an increase of both the active form of β-CATENIN and the expression of *LADON* (Figure 3J).

Taken together, these results show that *LADON* expression is positively regulated by WNT/β-CATENIN signaling in the A375 melanoma cell line.

***LADON* promotes A375 motility by inhibiting the expression of the metastasis suppressor NDRG1**

To identify factors acting downstream of *LADON* in A375 cells, we performed a proteomic analysis, looking for proteins that were differentially expressed between A375 cells and A375ΔE2 cells. The results are displayed in a volcano plot (Figure 4A). We focused on proteins that were identified by at least 2 independent peptides and with a fold change superior to 1.5. A Gene Ontology (GO) term analysis of the 28 proteins thus obtained, showed a significant enrichment in proteins involved in the composition of filamentous actin (PDLIM4, FREMT2 and NCKAP1), stress fibers (PDLIM4, Dynactin and FREMT2), as well as lamellipodia (PDLIM4, PLCG1, FREMT2 and NCKAP1) (Figure 4A; Table 1A). All of these were upregulated in mutant cells, suggesting a repressive role of *LADON* on their expression. Six proteins had a fold change superior to 2 (Table 1B), 5 of which were overexpressed in A375ΔN2cells. Interestingly, these overexpressed proteins turned out to be known tumor (FAM107B, ACPP) or metastasis (NDRG1) suppressors (Guo et al. 2017; Meeusen and Janssens 2018; Sharma et al. 2017), or transcription factors known to activate these proteins (p65, also known as NF-κB regulatory subunit RELA, is an activator of ACPP) (Zelivianski, Glowacki, and Lin 2004). Conversely, the under-expressed protein PPP4R2 is a regulatory subunit of PPP4C, which is known to promote cancer cell growth and invasion when over-

expressed (Hastie et al. 2000; Li et al. 2015). We focused our attention on NDRG1 (N-MYC downstream regulated gene 1), its activity as a metastasis suppressor in a number of cancers, including colon, prostate and breast cancers, being the most extensively characterized of the lot (Sun, Zhang, Bae, et al. 2013).

WB analysis confirmed an increase of NDRG1 levels in A375ΔE2 cells compared to A375 cells, thus validating the results of our proteomic analysis (Figure 4B). *NDRG1* mRNA levels were also increased in mutant clones (Figure 4C), suggesting that *LADON* may regulate *NDRG1* at the transcriptional level. Since the regulation of *NDRG1* expression is under the negative control of *MYCN* (Li etal., 2003), we measured the expression of *MYCN* in A375ΔE2 clones and found that it was reduced (Figure 4C). Western blot analysis confirmed this result (Figure4B), also consistent with our earlier RT2 array analysis of A375 cells (Figure 3A), showing that *MYCN* expression levels were higher after 96h than after 24h of culture.

NDRG1 has been shown to inhibit actin filament polymerization, stress fiber assembly and cell migration via the RHO-associated, coiled-coil continuing protein kinase 1 (ROCK1)/ phosphorylated myosin light chain 2 (pMLC2) pathway in prostate and colorectal cancer cells (Sun, Zhang, Zheng, et al. 2013). We therefore measured the levels of the pMLC2 in A375ΔE2 clones, and found that they were reduced (Figure 4B), consistent with the activation of NDRG1. To confirm a possible role of *NDRG1* in the inhibition of invasiveness in A375ΔE2 clones, we knocked down its expression in these cells. Transfection of A375ΔE2 cells with siRNAs targeting *NDRG1* resulted in a dramatic decrease of its expression at both mRNA and protein levels (Figure 4D and 4E), which was associated with the expected activation of pMLC2 (Figure 4E). Most importantly, the speed at which A375ΔE2cells filled the gap in a wound-healing assay increased significantly when *NDRG1* expression was knocked down (Figure 4F and 4G), confirming it as a key inhibitor of their motility.

In proliferating A375 cells, *MYCN* and *NDRG1* showed significant changes in their expression levels only after 72h of culture (Figure 4H), well after *LADON* expression started to increase, an observation consistent with the possibility that they depended on this increase. To find out whether this was the case, we treated A375 cells with 60 ng/ml of WNT3A. In this situation, where *LADON* is upregulated (Figure 3F), we obtained an increase of *MYCN* expression and a decrease of that of *NDRG1*, as expected (Figure 4I). The effect of WNT3A on *MYCN* and *NDRG1* expression was lost in A375ΔE2 cells (Figure 4I), while *AXIN2* expression was still activated (Figure 4J), confirming that *LADON* is required to modulate the expression of *MYCN* and *NDRG1* in the A375 cell line. We then knocked down *LADON* expression in the A375 cell line to assess the extent to which *MYCN* and *NDRG1* depend on it, using the same siRNAs as before. RT-qPCR results showed that a significant decrease of *LADON* expression led to a decrease of *MYCN* expression and an increase of *NDRG1* expression. In contrast, over-expression of the full-length *LADON* transcript in A375 cells or in A375ΔE2 clones resulted in the opposite effect (Figure 4L).

Taken together these results are consistent with *LADON* promoting the MAT and cell motility in the metastatic melanoma cell line A375 via an increase in *MYCN* expression, which in turn inhibits that of *NDRG1*.

Discussion

Our investigations into the mode of action of *NODAL* in metastatic melanoma cells found no evidence that this signaling molecule could influence their behavior *in vitro*, but revealed instead their reliance on the expression of *LADON*, a natural *NODAL* antisense transcript. Melanoma cells produce signals that induce changes in neighboring cells, and respond themselves to such signals by adopting a more invasive phenotype, all of which favors tumor progression. Our results show that *LADON* is involved in the mechanisms underlying how cells both produce these signals and respond to them. We found that *LADON* expression in A375 cells increases upon stimulation with A375-conditioned medium, promotes the mesenchymal to amoeboid transition associated with their acquisition of an invasive behavior, and also contributes to the potency of their conditioned medium. The increase in *LADON* expression is dependent on WNT/β-CATENIN signaling. It triggers an increase in *MYCN* expression, which results, via a regulatory cascade involving NDRG1, in the activation of pMLC2, a biochemical event known to underlie changes in cell shape and migratory behavior such as those we observed (Figure 5). Although the mode of action of *LADON* has to be ascertained, our findings support a critical role for its transcript in the network of interactions that governs tumor progression and metastasis.

The absence of *NODAL* transcripts in melanoma cell lines reported here is consistent with the results of other studies (Donovan et al., 2017; Strizzi et al., 2012), as well as with a recent characterization of transcript diversity at the human *NODAL* locus (Findlay and Postovit 2018). This last report and our own study show that most exon2-containing RNA species present in melanoma cells are in fact transcribed from the strand opposite to *NODAL*, and correspond to *LADON*. This finding explains some of the inconsistencies found in previous studies of the role of *NODAL* in melanoma, as an exon2-based assay had been used to track the expression of the gene in several of them (Findlay and Postovit 2018; Hardy et al., 2010; Postovit et al., 2008; Strizzi et al., 2012). The fact that *LADON* expression was mistaken for that of *NODAL* was compounded by the use of commercial antibodies cross-reacting with non-specific proteins that were erroneously identified as NODAL, as was later demonstrated (Donovan et al., 2017). This last study makes the claim that while there is evidence that the TGFβ and ACTIVIN-A ligands, both signaling via SMAD2,3, do promote tumor progression in melanoma in various ways, no such case can be made for NODAL. Further investigations are necessary to clarify how approaches specifically targeting *NODAL* gene products (transcript or ligand) in melanoma cells, where we now know that the gene is not expressed, nevertheless appeared to elicit an effect (reviewed in Findlay and Postovit 2018).

The absence of *NODAL* expression over the course of our 96h cultures means that the changes in behavior we characterized in A375 cells deleted for *NODAL* exon2, the failure to fill the gap in the scratch-wound assay, the failure to complete MAT, and the loss in invasiveness, result from the impact of the deletion on the expression of genes other than

NODAL. The only disturbance we could identify in the expression of the various transcription units in the vicinity of exon2 was that of *LADON*, which expressed a truncated transcript that could no longer be induced. The knockdown of *LADON* with specific siRNAs resulted in a similar loss of invasiveness as its deletion. It also led to an increase in cell proliferation, which implied that the failure of exon2-deleted cells to close the gap resulted from a drastic loss of motility that was not compensated by the gain in cell number. Finally, the forced expression of *LADON* in exon2-deleted cells restored the expression of *MYCN* and *NDRG1*, key agents of the transition disabled by the deletion, to levels closer to what they were in unmodified cells. These results show that *LADON* is implicated in the transition from a proliferative cell identity to a less proliferative but more invasive cell identity, a change of phenotype inherent to the metastatic process in melanoma (Carreira et al., 2006; Hoek et al., 2006; Hoek et al., 2008).

The demonstration that the increase in *LADON* expression triggers the down-regulation of the metastasis suppressor *NDRG1* is an important finding of this study. The fact that this increase is dependent on WNT/β-CATENIN signaling is intriguing. While this signaling pathway is known to promote metastasis in various cancers, notably carcinomas, understanding its role in melanoma has been more challenging. This may relate to the role of the pathway being already quite different in the motile melanocytes and in the tightly bound epithelial cells in which melanoma and carcinomas respectively originate (Gallagher et al., 2013). There is evidence of WNT/β-CATENIN signaling either promoting (Damsky et al. 2011; Eichhoff et al. 2011; Murakami et al. 2001; Sinnberg et al. 2011) or suppressing (Arozarena et al. 2011; Bachmann et al. 2005; Biechele et al. 2012; Chien et al. 2009; Kageshita et al. 2001; Maelandsmo et al. 2003) melanoma tumor progression. Confusingly, studies relying like ours on the A375 cell line drew what appear to be opposite conclusions on the role of WNT/β-CATENIN signaling in melanoma (Biechele et al. 2012; Grossmann et al. 2013). Yet there are striking similarities between their results and our own. Biechele et al. show that an increase in β-CATENIN signaling promotes apoptosis and an associated reduction in melanoma cell proliferation. This is consistent with our finding that cell proliferation is increased in *LADON*-depleted cells. Grossmann et al. show that an increase in β-CATENIN transcriptional activity stimulates tumor cell invasion, a result again consistent with the link we established between β-CATENIN signaling, the increase in *LADON* expression and an invasive phenotype. These results may not be valid for all melanomas, as discrepancies between other melanoma studies were explained by context-dependent differences, such as the presence of distinct downstream effectors of the pathway (Eichhoff et al. 2011; Widlund et al. 2002), a consequence of different melanomas following different paths. A study relying on a panel of melanoma cell lines that did not include A375 found, both *in vitro* and *in vivo*, that β-CATENIN inhibited their migration but nevertheless promoted melanoma metastasis (Gallagher et al., 2013). Whether it is suppressing or promoting its progression, the importance of WNT/β-CATENIN signaling in melanoma is not

in doubt. As a target of the pathway and a regulator of downstream oncogenes and tumor suppressors, *LADON* could provide a valuable point of entry for approaches aimed at derailing metastatic processes. It will be important in future studies to find out whether *LADON* is also a target of WNT/β-CATENIN signaling in other cancers where the pathway is known to play an important role in tumor progression.

Long-non-coding RNAs (lncRNAs) can regulate the expression of genes in their vicinity or at more distant loci (Kopp and Mendell 2018). Their action can take place in the nucleus or in the cytoplasm, and relies on their interaction with specific proteins, RNAs and regulatory elements. Natural antisense transcripts (NATs) constitute a class of lncRNAs. Their sequence overlaps with that of a protein-coding gene and is transcribed in the opposite direction (Rosikiewicz and Makałowska 2016; Werner 2013). This exonic overlap often allows a NAT to modulate the expression of its protein-coding counterpart with unprecedented specificity. There are now multiple examples of the implication of lncRNAs in tissue physiology and in the misregulation of cellular processes, which often result in cancer (Huarte 2015; Iyer et al. 2015; Schmitt and Chang 2016). This implication is the reason for the interest that lncRNAs currently elicit as biomarkers for diagnostic and prognosis, but also as potential targets for therapy or as tools to correct defective gene expression underlying cancer and other pathologies (Slaby, Laga, and Sedlacek 2017; Wahlestedt 2013). How *LADON* is regulating the expression of its downstream effectors is as yet unclear. It takes 24h to detect a significant change in the expression of *MYCN* or *NDRG1* after that of *LADON* has been altered, a delay implying that this regulation may not involve a direct interaction between *LADON* and these effectors. Even at its peak the expression of *LADON* never reaches a level that would allow it to be an effective miRNA sponge (Denzler et al. 2014, 2016). An interesting feature of the transcript is the presence in its 3'region of the short interspersed elements (SINEs) Alu and MIR. SINEs are non-autonomous transposable elements that are ubiquitous in the human genome. Among these, Alu elements are the most abundant and are often found embedded in the 3' end of mRNAs. The presence of Alu elements in lncRNAs has been associated with the capacity of such transcripts to regulate RNA transcription, decay or splicing (Gong and Maquat 2011; Holdt et al. 2013; Hu, Wang, and Shan 2016), while the presence of other SINEs has been associated with the regulation of other processes, such as translation (Carrieri et al. 2012; Johnson and Guigó 2014). Interestingly, it has been shown in neuroblastoma cells that β-CATENIN signaling can modulate *MYCN* expression via its impact on the stability of the *MYCN* mRNA (Duffy et al. 2014). Further investigations will be necessary to assess whether it is the presence of SINEs in the *LADON* transcript that conditions its capacity to modulate the expression of *MYCN* expression, as well as that of other genes, in melanoma cells.

To conclude, we identified a specific role for *LADON* in the regulatory cascade that via MYCN and NDRG1 allows melanoma cells to become more invasive. However, the evidence gathered so far, notably its impact on the expression of known oncogenes and tumor

suppressors known to be associated with processes other than cell motility and invasiveness, suggests its implication in tumor progression is likely to be broader. Also, *LADON* expression is not specific to melanoma and it is detected in cell lines derived from other types of cancer. It is also present in different healthy human cell types and tissues, where we currently have no indication of its function. Most of these cells, whether cancerous or not, do not express *NODAL*, but some do, leaving open the possibility that in such cases *LADON* has the capacity to modulate NODAL signaling. Future studies of *LADON* will thus have to address its function and mode of action in a variety of contexts.

Material and Methods

Key Resource Table

REAGENT or RESOURCE	SOURCE	IDENTIFIER
Antibodies		
Polyclonal Bovine anti-Rabbit IgG-HRP	Santa Cruz Biotechnology	sc-2370
Goat Anti-Mouse IgG (H+L) Preroxidase Conjugated	PIERCE	31430
Monoclonal Rabbit Non-phospho β-CATENIN (Ser33/3Thr41)	Cell Signaling Technology	#8814
Monoclonal Mouse β-CATENIN	Santa Cruz Biotechnology	sc-7963
Monoclonal Mouse N-MYC	Santa Cruz Biotechnology	sc-53993
Polyclonal Rabbit α/β–TUBULIN	Cell Signaling Technology	#2148
Monoclonal Mouse GSK-3α/β	Santa Cruz Biotechnology	sc-7291
Monoclonal Mouse pGSK-3α/β	Santa Cruz Biotechnology	sc-81496
Polyclonal Rabbit NDRG1	Cell Signaling Technology	#5196
Monoclonal Mouse Anti-p-ERK1/2 (pT202/pY204.22A)	Santa Cruz Biotechnology	sc-136521
Monoclonal Mouse Anti-ERK1/2	Santa Cruz Biotechnology	sc-514302
Polyclonal Rabbit phospho-Myosin Light Chain 2 (Thr18/Ser19)	Cell Signaling Technology	#3674
Monoclonal Mouse Myosin Light Chain 2 mouse	Santa Cruz Biotechnology	sc-517244
Bacterial and Virus Strains		
DH5α competent cells	Thermo Fisher Scientific	
Chemicals, Peptides, and Recombinant Proteins		
NuPAGENovex 4-12% Bis-Tris Gel 1.0mm,	Life Technologies	NP0323BOX

PROTEASE INHIBITORS Complete, Mini, EDTA-free	Roche	11836170001
NuPAGE LDS Sample Buffer (4X) 10ml	Life Technologies	NP0007
NuPAGE Sample Reducing Agent (10X)	Life Technologies	
D-MEM/F-12 (1:1) (1X), liquid plus Glutamax,	Life Technologies	31331028
FBS Foetal Bovine Serum, Origin: E.U. Approved (South American)	Life Technologies	10270106
Penicillin/Streptomycin	Life Technologies	15140-148
Trypsin 0.5% EDTA	Thermo Fisher	25300054
DAPI (4', 6-diamidino-2-phenylindole)	Invitrogen Molecular Probes (Thermo Fisher)	#D1306
ACTIVIN	CELL guidance systems	GFM29
SB431542	Millipore	616461
Dharmafect 1	Dharmacon	T-2001
NODAL	Biotechne	1315-ND-025
WNT3a	CELL guidance systems	GFM77
IWR-1-endo	Santa-Cruz Biotechnologie	Sc-295215
Experimental Models: Cell Lines		
A375	American Type Culture Collection	cat# ATCC ® CRL-1619
Melanocyte	From Nathalie Andrieu	N/A
MNT1	From Lionel Larue	N/A
SLM8	From Manuelle Viguier	N/A
888Mel	From Alain Mauviel	N/A
Oligonucleotides		
Primers	See Table S1	N/A
ON-TARGETplus Non-targeting Control siRNAs	Dharmacon	D-001810-01-05
ON-TARGETplus NDRG1 siRNAs SMART pool	Dharmacon,see Table S1	L-010563-00-0005
ON-TARGETplus LADON siRNAs 1,2 and 3	Dharmacon, see Table S1	SO-2770618G
Recombinant DNA/Plasmids		
pcDNA3.1	Thermo Fisher Scientific	**V79520**

pcDNA3.1 GFP	Thermo Fisher Scientific	
pcDDA3.1 LADON full length	This paper	N/A
Critical Commercial Assays		
RT2 Profiler PCR Arrays	QIAGEN	PAHS-176ZG-4
SUPERSCRIPT III VILO (50 réactions)	Thermo Fisher Scientific	11755050
LightCycler® FastStart DNA Master SYBR Green I	Roche	12239264001
RiboCellin	EUROBIO	RC1000
Software and Algorithms		
Graph Prism	GraphPad Software	https://www.graphpad.com/scientific-software/prism/
Adobe Illustrator	Adobe	https://www.adobe.com/products/illustrator.html
Image J	Schneider et al., 2012	https://imagej.nih.gov/ij/
UCSC	UCSC	https://genome.ucsc.edu
Excel	Microsoft	Microsoft

Plasmids

pcDNA3.1 and GFP pcDNA 3.1 are from Thermo Fisher scientific. LADON corresponding to AK001176.1, 1725bp was synthetized and inserted in pCDN3.1 (Genscript).

Cell lines and cell culture

The melanoma cell line A375 was purchased from ATCC. The normal melanocyte cell line was kindly provided by Nathalie Andrieu (Centre de Recherches en Cancérologie de Toulouse). The SLM8 cell line, kindly provided by M Viguier, is derived from a lymph node metastasis. The MNT1 melanoma cell line was a gift from Lionel Larue (Institute Curie CNRS UMR3347, INSERM U1021, Institute Curie). The 888Mel cell line, a gift from A. Mauviel (Institut Curie/CNRS UMR 3347/INSERM U1021), is derived from the lung metastatic WM793 melanoma cell line. Cells were grown in DMEM/F12 Glutamax (Invitrogen, Cergy- Pontoise, France) supplemented with antibiotics and 10% fetal calf serum (FCS) in a 5% CO2 atmosphere.

To prepare conditioned medium, melanoma cell lines were seeded at 70% confluence and then incubated for 72h in DMEM medium with or without FCS, as stated. This melanoma-conditioned medium was collected, centrifuged at 11000g for 15 min to remove cell debris and stored at -80°C.

The source and identifier of all the plasmids and cell lines are listed in the Key Resources Table.

Transmigration

Melanoma cells $1x10^5$ were seeded on the upper compartments of 2 mg／ml type I collagen-coated culture inserts (8 μm pores -Greiner Bio-One SAS, Courtaboeuf, France). DMEM supplemented with 10% FCS was used as a chemoattractant. A375 and A375E2 cells were allowed to migrate at 37°C and 5% CO2 for 24h00. Non-migrating cells on the upper face of the filter were removed by gently scraping them off using a cotton swab. Cells on the lower face were washed in PBS, fixed with 4% formaldehyde for 10 min and washed in PBS. Nuclei were then labeled with Hoechst for 5 min and washed again. Migrating cells were observed under an epifluorescence microscope using a 10x magnification. Five to ten pictures of adjacent fields of the central zone of each Transwell were taken. Fluorescence was quantified with the IMAGEJ software (US National Institutes of Health, Bethesda, MD, USA). Histograms display the data obtained from three independent experiments, and all the experiments were performed in duplicate. P-values were calculated by means of an ANOVA. Data are displayed as normalized results, where the nuclei of melanoma cells are set to 1 (or 100%) when grown in control condition.

A375 staining

For immunofluorescence experiments, A375 cells were seeded onto glass coverslips in twelve-well plates and incubated overnight. Next, cells were fixed in 4% formaldehyde solution and incubated with Alexa Fluor 647-coupled phalloidin to visualize F-actin, and Hoechst 33342 to label nuclei. Cover slips were then further washed in PBS, treated with Fluoromount-G anti-fade (Southern Biotech), and analyzed by confocal microscopy. The shape of A375 cells (n>20), elongated or round, was analyzed by IMAGEJ software, and the proportion of each corresponding cell type was quantified.

Wound healing/scratch assay

Cell migration was examined using a wound-healing assay. In brief, 0.2×10^6 cells were seeded in a well of twelve-well plates and at confluence a scratch wound was made with a 10 µl pipette tip, and then washed twice with PBS to remove cell debris. Wells were photographed under phase-contrast microscopy (time=0) while cells were allowed to migrate into the scratch wound area for up to 18h at 37°C 5% C02 atmosphere using an Essenbio IncuCyte apparatus. Speed of closure area was calculated overtime by IMAGEJ software. Data are represented as a ratio of migratory cells normalized to A375 cells migration in control condition. All experiments were performed in duplicate.

Western blot

Briefly, cells were lysed using RIPA buffer (50 mMTris–HCl, 10 mM $MgCl_2$, 20% Glycerol and 1% Triton X-100) containing protease and phosphatase inhibitors (Roche). Protein concentration was determined by BCA assay (Pierce) and 10-30 µg used for Western blot analysis. Western blot samples were combined with NuPAGE LDS sample buffer (Life Technologies) containing 0.05% β-mercaptoethanol, incubated at 95°C for 5 minutes and then resolved on SDS-PAGE (12% acrylamide). The resolved proteins were blotted onto nitrocellulose membrane and blocked with 5% milk or BSA (weight/volume). These were then incubated with primary antibodies overnight at 4°C, followed by an incubation at room

temperature with the respective horseradish peroxidase-conjugated secondary antibodies for 30 minutes. Details of the antibodies used are shown in the 'antibodies and reagents' section. Immunoreactive proteins were detected by enhanced chemiluminescence using a ChemiDoc XRS Molecular Imager (BioRad). Blots were quantified using the software available with this instrument. For all figures, representative blots are shown from replicate experiments.

CRISPR/CAS9 Genome Editing.

CRISPR/Cas9 genome editing was performed with GeneArt CRISPR Nuclease Vector Kit according to manufacturer's instructions (Life Technology). To select the target sequence for genome editing, the genomic sequences surrounding *NODAL* exon2 were submitted to an online CRISPR Design Tool (http://crispr.mit.edu/). Two target sites were selected upstream and downstream of this sequence. The oligonucleotides used to construct gRNAs for the human *NODAL* gene exon2 (deletion of 698 pb) are listed in Table S1.

The ds oligonucleotides generated were cloned into the GeneArt CRISPR Nuclease Vector. Competent E. coli cells were transfected with 3 µL of ligation reaction, and then 50 µL from the transformation reaction was spread on a pre-warmed LB agar plate containing 100 µg/mL ampicillin. Plates were incubated overnight at 37°C. The identity of the ds oligonucleotide insert in positive transformants was confirmed by sequencing. For A375 cell line transfection, the cationic lipid-based Lipofectamine 2000 Reagent was used. A375 cells positive for the transfection were sorted by FACS using OFP, a fluorescent protein present in the GeneArt CRISPR Nuclease Vector. Genotyping was performed on 96 clones to detect the deletion. Primers used to assess the efficacy of the CRISPR/Cas9 deletion are listed in Table S1.

Length of non-deleted amplicon: 1141 pb

Length of deleted amplicon: 445 pb

siRNAs

siRNAs against NDRG1 (mix of 4), LADON (two independents) and negative-control RNA were chemically synthesized (Dharmacon Research, Lafayette, USA). Synthetic siRNAs were transfected with Ribocellin Transfection Reagent (Eurobio) according to the manufacturer's instructions.

RNA extraction, reverse transcription (RT) and Quantitative PCR (Q-PCR)

For PCR analysis, 10^5 transfected GFP-positive cells were sorted by FACS analysis and collected into RNAse-free tubes. Total RNA extraction, cDNA synthesis and Q-PCR were performed as described previously (Legent K, et al 2006). For each gene and for a given RT PCR, values were normalized to the level of expression of the reference genes *RLP13* and *GAPDH*. No significant differences in the final ratio were found between the two reference genes; therefore, only *RPL13* was used for normalization. Primers and annealing temperatures for all genes are indicated in Table S1. For each gene, the values were averaged over at least three independent measurements. Three independent RNA isolations were performed for all experiments.

Sequences for all siRNAs and oligos used in this study can be found in Table S1.

RT² Profiler PCR Array-

The Human Cancer Stem Cells RT² Profiler PCR Array from Qiagen was used to profile the expression of 84 genes linked to cancer stem cells (CSCs) in the A375 cell line after 24h and 96h of culture, according to the manufacturer's instructions.

LC-MS/MS acquisition

For proteomics analysis two A375E2 clones (a and d) and two parental clones (A375a and b) were used.

Protein extracts (60µg) were precipitated with acetone at -20°C; the protein extracts were then incubated overnight at 37°C with 20 µl of 25mM NH_4HCO_3 containing sequencing-grade trypsin (12.5µg/ml, Promega). The resulting peptides were desalted using ZipTip µ-C18 Pipette Tips (Millipore) and analyzed either in technical triplicates or individually by a Q-Exactive Plus coupled to a Nano-LC Proxeon 1000 equipped with an easy spray ion source (all from Thermo Scientific). Peptides were separated by chromatography with the following parameters: Acclaim PepMap100 C18 pre-column (2cm, 75µm i.d., 3µm, 100Å), Pepmap-RSLC Proxeon C18 column (50cm, 75µm i.d., 2µm, 100 Å), 300 nl/min flow rate, gradient from 95 % solvent A (water, 0.1% formic acid) to 35% solvent B (100% acetonitrile, 0.1% formic acid) over a period of 98 min, followed by a column regeneration for 23 min, giving a total run time of 2 hrs. Peptides were analyzed in the Orbitrap cell, in full ion scan mode, at a resolution of 70,000 (at *m/z* 200), with a mass range of *m/z*375-1500 and an AGC target of $3x10^6$. Fragments were obtained by high collision-induced dissociation (HCD) activation with a collisional energy of 30%, and a quadrupole isolation window of 1.4 Da. MS/MS data were acquired in the Orbitrap cell in a Top20 mode, at a resolution of 17,500 with an AGC target of $2x10^5$, with a dynamic exclusion of 30 sec. MS/MS of most intense precursor were firstly acquired. Monocharged peptides and peptides with unassigned charge states were excluded from the MS/MS acquisition. The maximum ion accumulation times were set to 50 ms for MS acquisition and 45 ms for MS/MS acquisition.

LC-MS/MS data processing

The LC-MS/MS .raw files were processed using the Mascot search engine (version 2.5.1) coupled to Proteome Discoverer 2.2 (Thermo Fisher Scientific) for peptide identification with both a custom database and the database Swissprot (from 2017) with the *Homo sapiens* taxonomy. The following post-translational modifications were searched on proteome Discoverer 2.2: Oxidation of methionine, acetylation of protein N-term, phosphorylation of serine/threonine and phosphorylation of tyrosine. Peptide Identifications were validated using a 1% FDR (False Discovery Rate) threshold calculated with the Percolator algorithm.

Data collection and analysis

BigWig coverage files for the plus and minus strands were retrieved for the keratinocytes, fibroblasts and melanocytes in the skin02 sample (ENCODE project). The data retrieved from the National Center for Biotechnology Information Gene Expression Omnibus were accessible through GEO series number GSE78652 for A375cells, GSE16256 for H1 cells, GSE17312 for HUES64 cells, GSE90237 for MCF7, GSE88089 for HepG9, GSE78653 for HT1080, GSE78684 for HT-29, for the A375 melanoma line, H1 cells, HUES64 cells, MCF7, HepG2 cells, HT1080 and HT29, the bam files for the samples were first merged before deriving the bigWig coverage file.

The HG-U133 plus 2 arrays (Affymetrix) data presented are accessible through GEO Series accession GSE35388 analyzed by GEO2R at the National Center for Biotechnology Information Gene.

Statistical analysis

Data was collected and graphed using GraphPad Prism software. A 1-way ANOVA or two-sided student's t-test was used to determine statistical significance where appropriate. P-values of less than 0.05 were considered statistically significant. Information about the statistics used for each experiment, including sample size, experimental method, and specific statistic test employed, can be found in the relevant figures or figure legends.

Author Contributions

AD, JC, DF conceived the research. JC and DF obtained funding. JC and DF oversaw the experiments and data analysis. AD and DF carried out the experiments. AD analyzed the data. SD contributed to transmigration assays and RT-qPCR analysis. SC contributed to proteomic and genomic data analysis. CB contributed to PCR, RT-qPCR analysis and CRISPR cloning. SH contributed to WB analysis and manuscript editing. FD contributed to the transmigration assays and provided essential reagents and cell lines. JC, AD and DF wrote the manuscript.

Acknowledgements: We thank Nathalie Andrieu for the melanocyte cell line, Manuelle Viguier for the SLM8 cell line, Lionel Larue for the MNT1 cell line, Alain Mauviel for the 888Mel cell line and Delphine Delacour for antibodies. We thank Daniel Constam, Lionel Larue, Claire Rougeulle, Delphine Delacour and Vanessa Ribes for discussion and suggestions. We thank the Proteomics Core Facility at Institut Jacques Monod, notably T. Léger and C. Garcia, for the LC-MS/MS experiments, and the Région Ile-de-France (SESAME 2013 Q-Prot-B&M -LS093471), the Paris-Diderot University (ARS 2014-2018), and CNRS (Moyens d'Equipement Exceptionnel INSB 2015) for funding part of the LC-MS/MS equipment.

We also acknowledge the ImagoSeine Core Facility of Institut Jacques Monod, member of IBISA and of the France-Bioimaging (ANR-10-INBS-04) infrastructures.

Work in the Collignon lab was supported by grants from INCa (2014-1-PL BIO-01) and GEFLUC (2015-2017), and by Centre National de la Recherche Scientifique (CNRS).

Chiara BRESESTI was supported by the EUR G.E.N.E. (#ANR-17-EURE-0013), which is part of the Université de Paris IdEx (#ANR-18-IDEX-0001) funded by the French Government.

Competing interests: The authors declare no competing interests.

References

Arozarena, I., Bischof, H., Gilby, D., Belloni, B., Dummer, R., & Wellbrock, C. (2011). In melanoma, beta-catenin is a suppressor of invasion. *Oncogene*, *30*(45), 4531–4543. https://doi.org/10.1038/onc.2011.162

Bachmann, I. M. (2005). Importance of P-Cadherin, -Catenin, and Wnt5a/Frizzled for Progression of Melanocytic Tumors and Prognosis in Cutaneous Melanoma. *Clinical Cancer Research*, *11*(24), 8606–8614. https://doi.org/10.1158/1078-0432.CCR-05-0011

Bianco, C., Adkins, H. B., Wechselberger, C., Seno, M., Normanno, N., De Luca, A., Sun, Y., Khan, N., Kenney, N., Ebert, A., Williams, K. P., Sanicola, M., & Salomon, D. S. (2002). Cripto-1 Activates Nodal- and ALK4-Dependent and -Independent Signaling Pathways in Mammary Epithelial Cells. *Molecular and Cellular Biology*, *22*(8), 2586–2597. https://doi.org/10.1128/MCB.22.8.2586-2597.2002

Biechele, T. L., Kulikauskas, R. M., Toroni, R. A., Lucero, O. M., Swift, R. D., James, R. G., Robin, N. C., Dawson, D. W., Moon, R. T., & Chien, A. J. (2012). Wnt/β-catenin signaling and AXIN1 regulate apoptosis mediated by inhibition of BRAFV600E kinase in human melanoma. *Science Signaling*, *5*(206), ra3. https://doi.org/10.1126/scisignal.2002274

Bodenstine, T. M., Chandler, G. S., Reed, D. W., Margaryan, N. V., Gilgur, A., Atkinson, J., Ahmed, N., Hyser, M., Seftor, E. A., Strizzi, L., & Hendrix, M. J. C. (2016). Nodal expression in triple-negative breast cancer: Cellular effects of its inhibition following doxorubicin treatment. *Cell Cycle*, *15*(9), 1295–1302. https://doi.org/10.1080/15384101.2016.1160981

Carreira, S., Goodall, J., Denat, L., Rodriguez, M., Nuciforo, P., Hoek, K. S., Testori, A., Larue, L., & Goding, C. R. (2006). Mitf regulation of Dia1 controls melanoma proliferation and invasiveness. *Genes & Development*, *20*(24), 3426–3439. https://doi.org/10.1101/gad.406406

Carrieri, C., Cimatti, L., Biagioli, M., Beugnet, A., Zucchelli, S., Fedele, S., Pesce, E., Ferrer, I., Collavin, L., Santoro, C., Forrest, A. R. R., Carninci, P., Biffo, S., Stupka, E., & Gustincich, S. (2012). Long non-coding antisense RNA controls Uchl1 translation through an embedded SINEB2 repeat. *Nature*, *491*(7424), 454–457. https://doi.org/10.1038/nature11508

Chaffer, C. L., & Weinberg, R. A. (2011). A Perspective on Cancer Cell Metastasis. *Science*, *331*(6024), 1559–1564. https://doi.org/10.1126/science.1203543

Chien, A. J., Moore, E. C., Lonsdorf, A. S., Kulikauskas, R. M., Rothberg, B. G., Berger, A. J., Major, M. B., Hwang, S. T., Rimm, D. L., & Moon, R. T. (2009). Activated Wnt/ß-catenin signaling in melanoma is associated with decreased proliferation in patient tumors and a murine melanoma model. *MEDICAL SCIENCES*, 6.

Constam, D. B., & Robertson, E. J. (1999). Regulation of Bone Morphogenetic Protein Activity by Pro Domains and Proprotein Convertases. *Journal of Cell Biology*, *144*(1), 139–149. https://doi.org/10.1083/jcb.144.1.139

Costa. (2009). Effects of two organotin(IV)(sulfonatophenyl)porphinates on MAPKs and on the growth of A375 human melanoma cells. *Oncology Reports*. https://doi.org/10.3892/or_00000261

Damsky, W. E., Curley, D. P., Santhanakrishnan, M., Rosenbaum, L. E., Platt, J. T., Gould Rothberg, B. E., Taketo, M. M., Dankort, D., Rimm, D. L., McMahon, M., & Bosenberg, M. (2011). β-Catenin Signaling Controls Metastasis in Braf-Activated Pten-Deficient Melanomas. *Cancer Cell*, *20*(6), 741–754. https://doi.org/10.1016/j.ccr.2011.10.030

Denzler, R., Agarwal, V., Stefano, J., Bartel, D. P., & Stoffel, M. (2014). Assessing the ceRNA Hypothesis with Quantitative Measurements of miRNA and Target Abundance. *Molecular Cell*, *54*(5), 766–776. https://doi.org/10.1016/j.molcel.2014.03.045

Denzler, R., McGeary, S. E., Title, A. C., Agarwal, V., Bartel, D. P., & Stoffel, M. (2016). Impact of MicroRNA Levels, Target-Site Complementarity, and Cooperativity on Competing Endogenous RNA-Regulated Gene Expression. *Molecular Cell*, *64*(3), 565–579. https://doi.org/10.1016/j.molcel.2016.09.027

Donovan, P., Dubey, O. A., Kallioinen, S., Rogers, K. W., Muehlethaler, K., Müller, P., Rimoldi, D., & Constam, D. B. (2017). Paracrine Activin-A Signaling Promotes Melanoma Growth and Metastasis through Immune Evasion. *Journal of Investigative Dermatology*, *137*(12), 2578–2587. https://doi.org/10.1016/j.jid.2017.07.845

Duffy, D. J., Krstic, A., Schwarzl, T., Higgins, D. G., & Kolch, W. (2014). GSK3 Inhibitors Regulate MYCN mRNA Levels and Reduce Neuroblastoma Cell Viability through Multiple Mechanisms, Including p53 and Wnt Signaling. *Molecular Cancer Therapeutics*, *13*(2), 454–467. https://doi.org/10.1158/1535-7163.MCT-13-0560-T

Eichhoff, O. M., Weeraratna, A., Zipser, M. C., Denat, L., Widmer, D. S., Xu, M., Kriegl, L., Kirchner, T., Larue, L., Dummer, R., & Hoek, K. S. (2011). Differential LEF1 and TCF4 expression is involved in melanoma cell phenotype switching: LEF1/TCF4 switching in melanoma progression. *Pigment Cell & Melanoma Research*, *24*(4), 631–642. https://doi.org/10.1111/j.1755-148X.2011.00871.x

Ellis, P. S., Burbridge, S., Soubes, S., Ohyama, K., Ben-Haim, N., Chen, C., Dale, K., Shen, M. M., Constam, D., & Placzek, M. (2015). ProNodal acts via FGFR3 to govern duration of Shh expression in the prechordal mesoderm. *Development*, *142*(22), 3821–3832. https://doi.org/10.1242/dev.119628

Findlay, S. D., & Postovit, L.-M. (2018). Comprehensive characterization of transcript diversity at the human NODAL locus. *BioRxiv*, 254409. https://doi.org/10.1101/254409

Friedl, P., & Wolf, K. (2010). Plasticity of cell migration: A multiscale tuning model. *The Journal of Cell Biology*, *188*(1), 11–19. https://doi.org/10.1083/jcb.200909003

Gadea, G., de Toledo, M., Anguille, C., & Roux, P. (2007). Loss of p53 promotes RhoA-ROCK-dependent cell migration and invasion in 3D matrices. *The Journal of Cell Biology*, *178*(1), 23–30. https://doi.org/10.1083/jcb.200701120

Gong, C., & Maquat, L. E. (2011). LncRNAs transactivate STAU1-mediated mRNA decay by duplexing with 3′ UTRs via Alu elements. *Nature*, *470*(7333), 284–288. https://doi.org/10.1038/nature09701

Grossmann, A. H., Yoo, J. H., Clancy, J., Sorensen, L. K., Sedgwick, A., Tong, Z., Ostanin, K., Rogers, A., Grossmann, K. F., Tripp, S. R., Thomas, K. R., Odelberg, S. J., & Li, D. Y. (n.d.). *The Small GTPase ARF6*

Stimulates b-Catenin Transcriptional Activity During WNT5A-Mediated Melanoma Invasion and Metastasis. 14.

Guo, J., Bian, Y., Wang, Y., Chen, L., Yu, A., & Sun, X. (2017). *FAM107B* is regulated by *S100A4* and mediates the effect of *S100A4* on the proliferation and migration of MGC803 gastric cancer cells: *FAM107B* mediates effect of *S100A4* in MGC803 cells. *Cell Biology International*, *41*(10), 1103–1109. https://doi.org/10.1002/cbin.10816

Hardy, K. M., Kirschmann, D. A., Seftor, E. A., Margaryan, N. V., Postovit, L.-M., Strizzi, L., & Hendrix, M. J. C. (2010). Regulation of the embryonic morphogen Nodal by Notch4 facilitates manifestation of the aggressive melanoma phenotype. *Cancer Research*, *70*(24), 10340–10350. https://doi.org/10.1158/0008-5472.CAN-10-0705

Hastie, C. J., Carnegie, G. K., Morrice, N., & Cohen, P. T. (2000). A novel 50 kDa protein forms complexes with protein phosphatase 4 and is located at centrosomal microtubule organizing centres. *Biochemical Journal*, *347*(Pt 3), 845–855.

Hoek, K. S., Eichhoff, O. M., Schlegel, N. C., Dobbeling, U., Kobert, N., Schaerer, L., Hemmi, S., & Dummer, R. (2008). In vivo Switching of Human Melanoma Cells between Proliferative and Invasive States. *Cancer Research*, *68*(3), 650–656. https://doi.org/10.1158/0008-5472.CAN-07-2491

Hoek, Keith S., Schlegel, N. C., Brafford, P., Sucker, A., Ugurel, S., Kumar, R., Weber, B. L., Nathanson, K. L., Phillips, D. J., Herlyn, M., Schadendorf, D., & Dummer, R. (2006). Metastatic potential of melanomas defined by specific gene expression profiles with no BRAF signature. *Pigment Cell Research*, *19*(4), 290–302. https://doi.org/10.1111/j.1600-0749.2006.00322.x

Holdt, L. M., Hoffmann, S., Sass, K., Langenberger, D., Scholz, M., Krohn, K., Finstermeier, K., Stahringer, A., Wilfert, W., Beutner, F., Gielen, S., Schuler, G., Gäbel, G., Bergert, H., Bechmann, I., Stadler, P. F., Thiery, J., & Teupser, D. (2013). Alu Elements in ANRIL Non-Coding RNA at Chromosome 9p21 Modulate Atherogenic Cell Functions through Trans-Regulation of Gene Networks. *PLoS Genetics*, *9*(7), e1003588. https://doi.org/10.1371/journal.pgen.1003588

Hu, S., Wang, X., & Shan, G. (2016). Insertion of an Alu element in a lncRNA leads to primate-specific modulation of alternative splicing. *Nature Structural & Molecular Biology*, *23*(11), 1011–1019. https://doi.org/10.1038/nsmb.3302

Huarte, M. (2015). The emerging role of lncRNAs in cancer. *Nature Medicine*, *21*(11), 1253–1261. https://doi.org/10.1038/nm.3981

Iyer, M. K., Niknafs, Y. S., Malik, R., Singhal, U., Sahu, A., Hosono, Y., Barrette, T. R., Prensner, J. R., Evans, J. R., Zhao, S., Poliakov, A., Cao, X., Dhanasekaran, S. M., Wu, Y.-M., Robinson, D. R., Beer, D. G., Feng, F. Y., Iyer, H. K., & Chinnaiyan, A. M. (2015). The landscape of long noncoding RNAs in the human transcriptome. *Nature Genetics*, *47*(3), 199–208. https://doi.org/10.1038/ng.3192

Jho, E., Zhang, T., Domon, C., Joo, C.-K., Freund, J.-N., & Costantini, F. (2002). Wnt/beta-catenin/Tcf signaling induces the transcription of Axin2, a negative regulator of the signaling pathway. *Molecular and Cellular Biology*, *22*(4), 1172–1183. https://doi.org/10.1128/mcb.22.4.1172-1183.2002

Johnson, R., & Guigo, R. (2014). The RIDL hypothesis: Transposable elements as functional domains of long noncoding RNAs. *RNA*, *20*(7), 959–976. https://doi.org/10.1261/rna.044560.114

Kageshita, T., Hamby, C. V., Ishihara, T., Matsumoto, K., Saida, T., & Ono, T. (2001). Loss of beta-catenin expression associated with disease progression in malignant melanoma. *British Journal of Dermatology*, *145*(2), 210–216. https://doi.org/10.1046/j.1365-2133.2001.04336.x

Kim, D. S., Lee, M. W., Lee, T.-H., Sung, K. W., Koo, H. H., & Yoo, K. H. (2017). Cell culture density affects the stemness gene expression of adipose tissue-derived mesenchymal stem cells. *Biomedical Reports*, *6*(3), 300–306. https://doi.org/10.3892/br.2017.845

Kopp, F., & Mendell, J. T. (2018). Functional Classification and Experimental Dissection of Long Noncoding RNAs. *Cell*, *172*(3), 393–407. https://doi.org/10.1016/j.cell.2018.01.011

Le Good, J. A., Joubin, K., Giraldez, A. J., Ben-Haim, N., Beck, S., Chen, Y., Schier, A. F., & Constam, D. B. (2005). Nodal stability determines signaling range. *Current Biology : CB*, *15*(1), 31–36. https://doi.org/10.1016/j.cub.2004.12.062

Li, J., & Kretzner, L. (2003). The growth-inhibitory Ndrg1 gene is a Myc negative target in human neuroblastomas and other cell types with overexpressed N- or c-myc. *Molecular and Cellular Biochemistry*, *250*(1–2), 91–105. https://doi.org/10.1023/a:1024918328162

Li, X., Liang, L., Huang, L., Ma, X., Li, D., & Cai, S. (2015). High expression of protein phosphatase 4 is associated with the aggressive malignant behavior of colorectal carcinoma. *Molecular Cancer*, *14*(1), 95. https://doi.org/10.1186/s12943-015-0356-7

Lim, S., Kumari, P., Gilligan, P., Quach, H. N. B., Mathavan, S., & Sampath, K. (2012). Dorsal activity of maternal squint is mediated by a non-coding function of the RNA. *Development*, *139*(16), 2903–2915. https://doi.org/10.1242/dev.077081

Ma, L., Young, J., Prabhala, H., Pan, E., Mestdagh, P., Muth, D., Teruya-Feldstein, J., Reinhardt, F., Onder, T. T., Valastyan, S., Westermann, F., Speleman, F., Vandesompele, J., & Weinberg, R. A. (2010). MiR-9, a MYC/MYCN-activated microRNA, regulates E-cadherin and cancer metastasis. *Nature Cell Biology*, *12*(3), 247–256. https://doi.org/10.1038/ncb2024

Mælandsmo, G. M., Holm, R., Nesland, J. M., Fodstad, Ø., & Flørenes, V. A. (2003). Reduced β-Catenin Expression in the Cytoplasm of Advanced-Stage Superficial Spreading Malignant Melanoma. *Clinical Cancer Research*, *9*(9), 3383–3388.

Meeusen, B., & Janssens, V. (2018). Tumor suppressive protein phosphatases in human cancer: Emerging targets for therapeutic intervention and tumor stratification. *The International Journal of Biochemistry & Cell Biology*, *96*, 98–134. https://doi.org/10.1016/j.biocel.2017.10.002

Murakami, T., Toda, S., Fujimoto, M., Ohtsuki, M., Byers, H. R., Etoh, T., & Nakagawa, H. (2001). Constitutive Activation of Wnt/β-Catenin Signaling Pathway in Migration-Active Melanoma Cells: Role of LEF-1 in Melanoma with Increased Metastatic Potential. *Biochemical and Biophysical Research Communications*, *288*(1), 8–15. https://doi.org/10.1006/bbrc.2001.5719

Ota, T., Suzuki, Y., Nishikawa, T., Otsuki, T., Sugiyama, T., Irie, R., Wakamatsu, A., Hayashi, K., Sato, H., Nagai, K., Kimura, K., Makita, H., Sekine, M., Obayashi, M., Nishi, T., Shibahara, T., Tanaka, T., Ishii, S., Yamamoto, J., … Sugano, S. (2004). Complete sequencing and characterization of 21,243 full-length human cDNAs. *Nature Genetics*, *36*(1), 40–45. https://doi.org/10.1038/ng1285

Panková, K., Rösel, D., Novotný, M., & Brábek, J. (2010). The molecular mechanisms of transition between mesenchymal and amoeboid invasiveness in tumor cells. *Cellular and Molecular Life Sciences: CMLS*, *67*(1), 63–71. https://doi.org/10.1007/s00018-009-0132-1

Papageorgiou, I., Nicholls, P. K., Wang, F., Lackmann, M., Makanji, Y., Salamonsen, L. A., Robertson, D. M., & Harrison, C. A. (2009). Expression of nodal signalling components in cycling human endometrium and in endometrial cancer. *Reproductive Biology and Endocrinology : RB&E*, *7*, 122. https://doi.org/10.1186/1477-7827-7-122

Postovit, L.-M., Margaryan, N. V., Seftor, E. A., Kirschmann, D. A., Lipavsky, A., Wheaton, W. W., Abbott, D. E., Seftor, R. E. B., & Hendrix, M. J. C. (2008). Human embryonic stem cell microenvironment suppresses the tumorigenic phenotype of aggressive cancer cells. *Proceedings of the National Academy of Sciences*, *105*(11), 4329–4334. https://doi.org/10.1073/pnas.0800467105

Quail, D. F., Siegers, G. M., Jewer, M., & Postovit, L.-M. (2013). Nodal signalling in embryogenesis and tumourigenesis. *The International Journal of Biochemistry & Cell Biology*, *45*(4), 885–898. https://doi.org/10.1016/j.biocel.2012.12.021

Robertson, E. J. (2014). Dose-dependent Nodal/Smad signals pattern the early mouse embryo. *Seminars in Cell & Developmental Biology*, *32*, 73–79. https://doi.org/10.1016/j.semcdb.2014.03.028

Rosikiewicz, W., & Makałowska, I. (2017). Biological Functions of Natural Antisense Transcripts. *Acta Biochimica Polonica*, *63*(4). https://doi.org/10.18388/abp.2016_1350

Sahai, E., & Marshall, C. J. (2003). Differing modes of tumour cell invasion have distinct requirements for Rho/ROCK signalling and extracellular proteolysis. *Nature Cell Biology*, *5*(8), 711–719. https://doi.org/10.1038/ncb1019

Sanz-Moreno, V., Gadea, G., Ahn, J., Paterson, H., Marra, P., Pinner, S., Sahai, E., & Marshall, C. J. (2008). Rac activation and inactivation control plasticity of tumor cell movement. *Cell*, *135*(3), 510–523. https://doi.org/10.1016/j.cell.2008.09.043

Sanz-Moreno, V., Gaggioli, C., Yeo, M., Albrengues, J., Wallberg, F., Viros, A., Hooper, S., Mitter, R., Féral, C. C., Cook, M., Larkin, J., Marais, R., Meneguzzi, G., Sahai, E., & Marshall, C. J. (2011). ROCK and JAK1 signaling cooperate to control actomyosin contractility in tumor cells and stroma. *Cancer Cell*, *20*(2), 229–245. https://doi.org/10.1016/j.ccr.2011.06.018

Schmitt, A. M., & Chang, H. Y. (2016). Long Noncoding RNAs in Cancer Pathways. *Cancer Cell*, *29*(4), 452–463. https://doi.org/10.1016/j.ccell.2016.03.010

Sharma, A., Mendonca, J., Ying, J., Kim, H.-S., Verdone, J. E., Zarif, J. C., Carducci, M., Hammers, H., Pienta, K. J., & Kachhap, S. (2017). The prostate metastasis suppressor gene NDRG1 differentially

regulates cell motility and invasion. *Molecular Oncology*, *11*(6), 655–669. https://doi.org/10.1002/1878-0261.12059

Sinnberg, T., Menzel, M., Ewerth, D., Sauer, B., Schwarz, M., Schaller, M., Garbe, C., & Schittek, B. (2011). β-Catenin Signaling Increases during Melanoma Progression and Promotes Tumor Cell Survival and Chemoresistance. *PLoS ONE*, *6*(8), e23429. https://doi.org/10.1371/journal.pone.0023429

Slaby, O., Laga, R., & Sedlacek, O. (2017). Therapeutic targeting of non-coding RNAs in cancer. *Biochemical Journal*, *474*(24), 4219–4251. https://doi.org/10.1042/BCJ20170079

Strizzi, L., Hardy, K. M., Kirschmann, D. A., Ahrlund-Richter, L., & Hendrix, M. J. C. (2012). Nodal Expression and Detection in Cancer: Experience and Challenges. *Cancer Research*, *72*(8), 1915–1920. https://doi.org/10.1158/0008-5472.CAN-11-3419

Sun, J., Zhang, D., Bae, D.-H., Sahni, S., Jansson, P., Zheng, Y., Zhao, Q., Yue, F., Zheng, M., Kovacevic, Z., & Richardson, D. R. (2013). Metastasis suppressor, NDRG1, mediates its activity through signaling pathways and molecular motors. *Carcinogenesis*, *34*(9), 1943–1954. https://doi.org/10.1093/carcin/bgt163

Taddei, M. L., Giannoni, E., Morandi, A., Ippolito, L., Ramazzotti, M., Callari, M., Gandellini, P., & Chiarugi, P. (2014). Mesenchymal to amoeboid transition is associated with stem-like features of melanoma cells. *Cell Communication and Signaling : CCS*, *12*, 24. https://doi.org/10.1186/1478-811X-12-24

Topczewska, J. M., Postovit, L.-M., Margaryan, N. V., Sam, A., Hess, A. R., Wheaton, W. W., Nickoloff, B. J., Topczewski, J., & Hendrix, M. J. C. (2006). Embryonic and tumorigenic pathways converge via Nodal signaling: Role in melanoma aggressiveness. *Nature Medicine*, *12*(8), 925–932. https://doi.org/10.1038/nm1448

Wahlestedt, C. (2013). Targeting long non-coding RNA to therapeutically upregulate gene expression. *Nature Reviews Drug Discovery*, *12*(6), 433–446. https://doi.org/10.1038/nrd4018

Werner, A. (2013). Biological functions of natural antisense transcripts. *BMC Biology*, *11*(1), 31. https://doi.org/10.1186/1741-7007-11-31

Widlund, H. R., Horstmann, M. A., Price, E. R., Cui, J., Lessnick, S. L., Wu, M., He, X., & Fisher, D. E. (2002). β-Catenin–induced melanoma growth requires the downstream target Microphthalmia-associated transcription factor. *Journal of Cell Biology*, *158*(6), 1079–1087. https://doi.org/10.1083/jcb.200202049

Xiao, D., Ohlendorf, J., Chen, Y., Taylor, D. D., Rai, S. N., Waigel, S., Zacharias, W., Hao, H., & McMasters, K. M. (2012). Identifying mRNA, MicroRNA and Protein Profiles of Melanoma Exosomes. *PLoS ONE*, *7*(10), e46874. https://doi.org/10.1371/journal.pone.0046874

Zelivianski, S. (2004). Transcriptional activation of the human prostatic acid phosphatase gene by NF-B via a novel hexanucleotide-binding site. *Nucleic Acids Research*, *32*(12), 3566–3580. https://doi.org/10.1093/nar/gkh677

Figure 1.

A

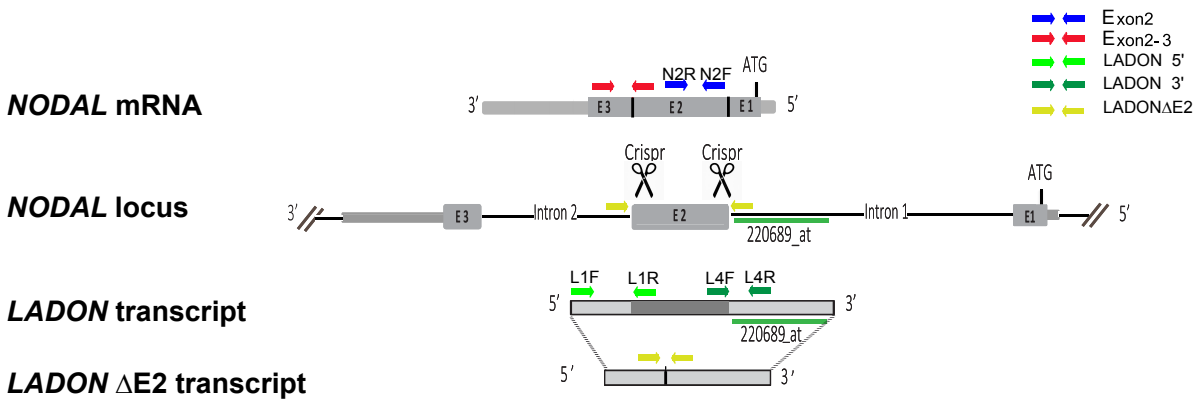

B

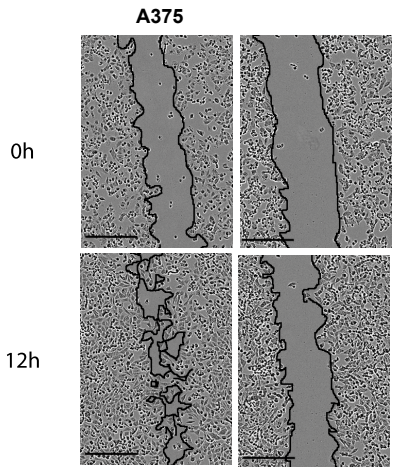

C

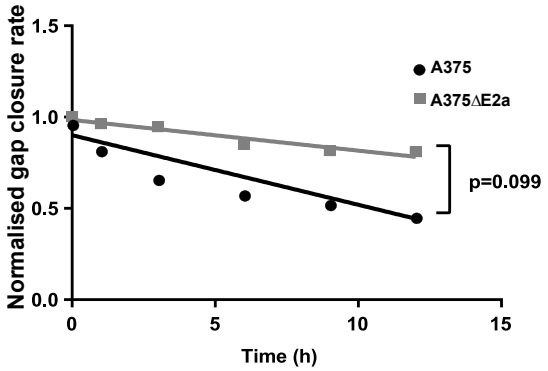

D

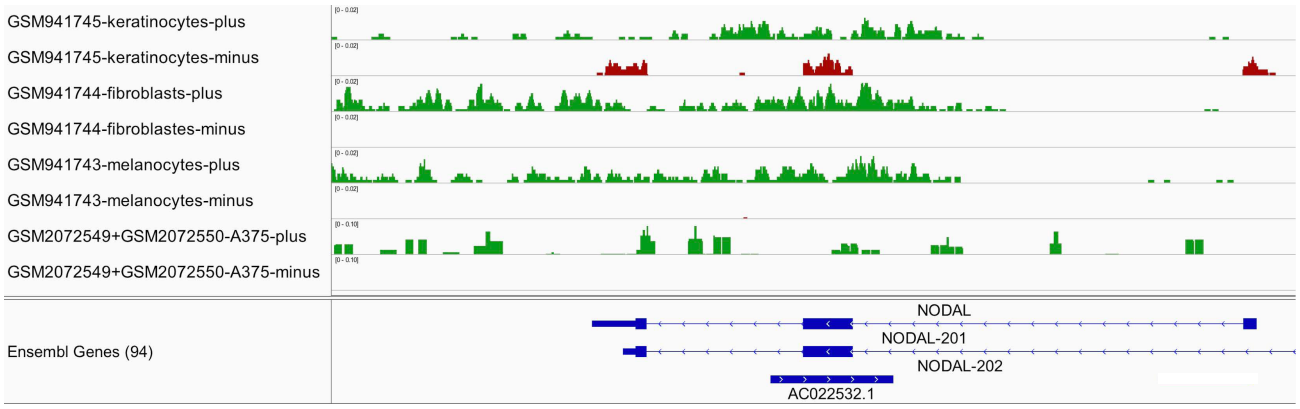

E

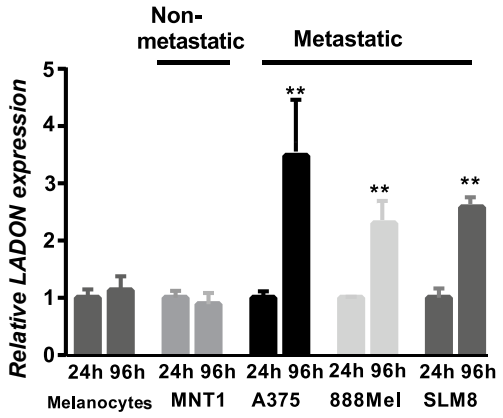

F

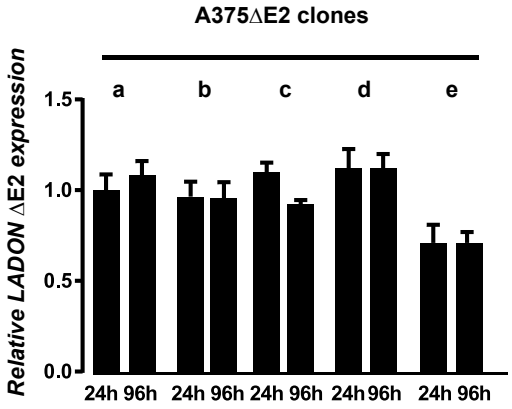

Figure 1. The invasive behavior of A375 cells is dependent on the presence of *NODAL* exon2.

(A) Schematic diagram of the human *NODAL* locus with its 3 exons (E1 to E3), showing the full-length *NODAL* mRNA above, and the *LADON* RNA transcribed from the opposite strand below. The *LADON-ΔE2* RNA is produced by cells where *NODAL* exon2 has been deleted via genome editing. Arrows represent the primers used to track these transcripts.
(B) Representative images, acquired at t=0 and t=12h, of scratch-wound healing assays performed with A375 and A375ΔE2a cells.
(C) Quantification of the normalized gap closure rate of A375 and A375ΔE2 cells during the scratch-wound healing assay shown in (B). The p-values were calculated by a two-way ANOVA test.
(D) Mapping of strand-specific expression data at the human *NODAL* locus in cell lines representative of skin cell types and in the A375 melanoma cell line. Read coverage is displayed in red for the minus strand (corresponding to *NODAL*) and in green for the plus strand (corresponding to *LADON*). The exonic structure of the two genes is shown below.
(E) RT-qPCR measurements of *LADON* expression were performed in melanocytes, non-metastatic (MNT1) or metastatic melanoma cells (A375, 888Mel and SLM8), after 24h and 96h of culture. *LADON* expression was normalized to that of endogenous *RPL13*. For each cell line its 24h value is then normalized to 1.
(F) RT-qPCR analysis of *LADON*-ΔE2 expression in five independent A375ΔE2 clones shows that it remains stable over the course of the culture.
Histograms in (E) and (F) display mean values from a minimum of three independent replicates. Error Bars indicate SD. The p-values were calculated by Student's t test from two independent experiments. $^{**}p < 0.01$.

Figure 2

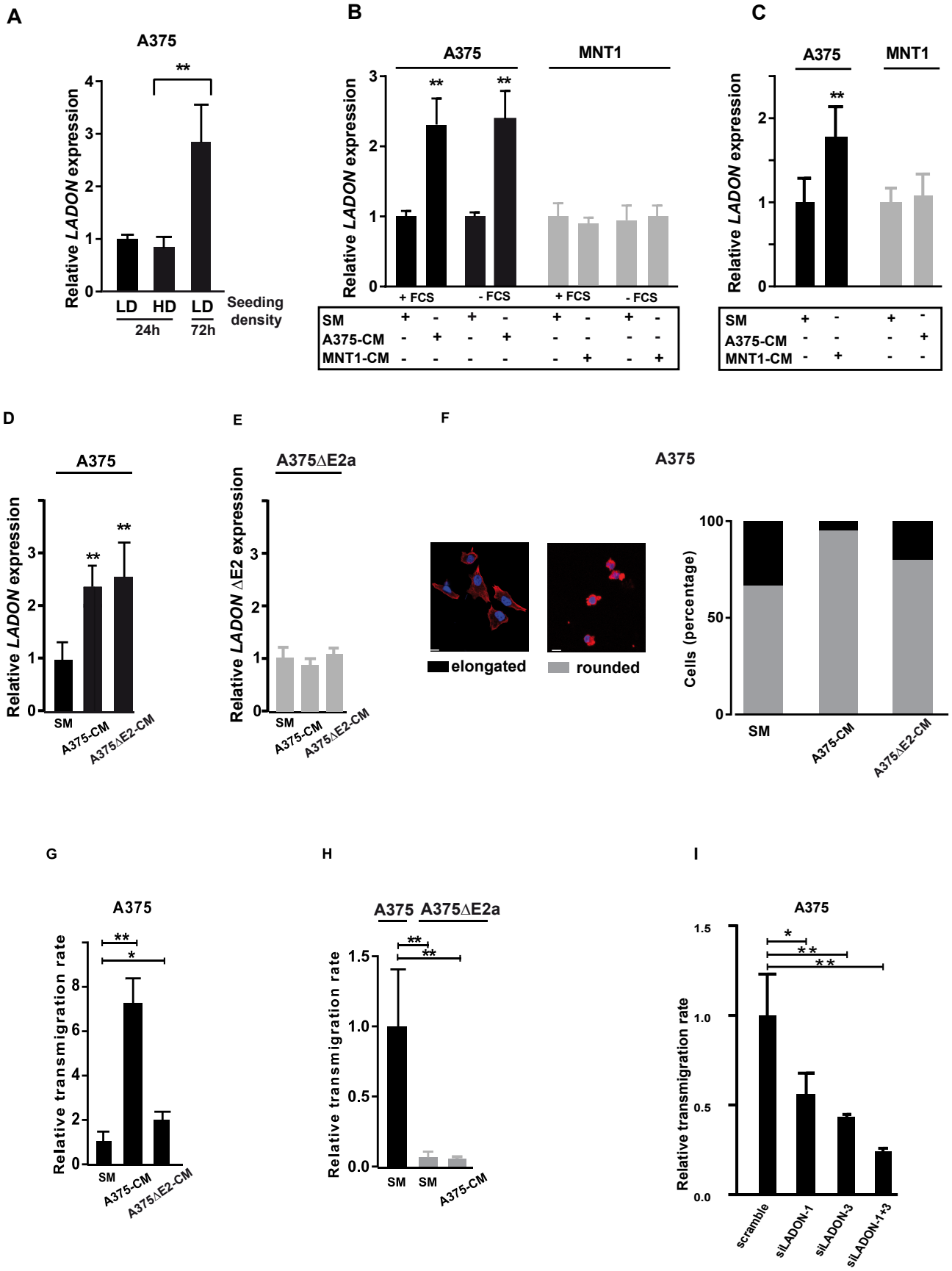
A
A375
Relative LADON expression
LD
HD
LD
24h
72h
Seeding density
B
A375
MNT1
Relative LADON expression
+ FCS
- FCS
+ FCS
- FCS
SM
A375-CM
MNT1-CM
C
A375
MNT1
Relative LADON expression
SM
A375-CM
MNT1-CM
D
A375
Relative LADON expression
SM
A375-CM
A375ΔE2-CM
E
A375ΔE2a
Relative LADON ΔE2 expression
SM
A375-CM
A375ΔE2-CM
F
A375
elongated
rounded
Cells (percentage)
SM
A375-CM
A375ΔE2-CM
G
A375
Relative transmigration rate
SM
A375-CM
A375ΔE2-CM
H
A375
A375ΔE2a
Relative transmigration rate
SM
SM
A375-CM
I
A375
Relative transmigration rate
scramble
siLADON-1
siLADON-3
siLADON-1+3

Figure 2. A375 cells secrete factors that promote *LADON* expression and invasion

(A) RT-qPCR analysis of *LADON* expression in A375 cells seeded at low (LD) or high density (HD) and cultured for 24 or 72h. Cell density does not affect *LADON*'s expression level whereas cell culture duration does.
(B, C) RT-qPCR analyses of *LADON* expression in A375 and MNT1 cells cultured for 24h in standard culture medium (SM), in A375-conditioned medium (A375-CM) or in MNT1-conditioned medium (MNT1-CM), with or without fetal calf serum (FCS).
(D, E) RT-PCR analysis of *LADON* and *LADON-ΔE2* expression in A375 cells cultured for 24h in SM, A375-CM or A375ΔE2-conditioned medium (A375ΔE2-CM).
(F) Representative images of A375 cells with elongated or rounded morphology, visualized after F-actin (red) and Hoechst 33342 (nuclear, blue) staining. Scale bar 25µm. The histogram shows the percentage of the two cell morphologies in A375 cells cultured for 24h in SM, A375-CM or A375ΔE2-CM.
(G, H) Relative transmigration rates of A375 or A375ΔE2a cells cultured in SM, A375-CM or A375ΔE2-CM.
(I) Relative transmigration rate of A375 cells in presence of scramble siRNA, siLADON-1, siLADON-3, or siLADON-1 and -3. Values obtained with the scramble siRNA were normalized to 1.
Histograms display mean values from a minimum of three independent replicates. Error Bars indicate SD. The p-values were calculated by Student's t test from two independent experiments. *$p < 0.05$, **$p < 0.01$.

Figure 3

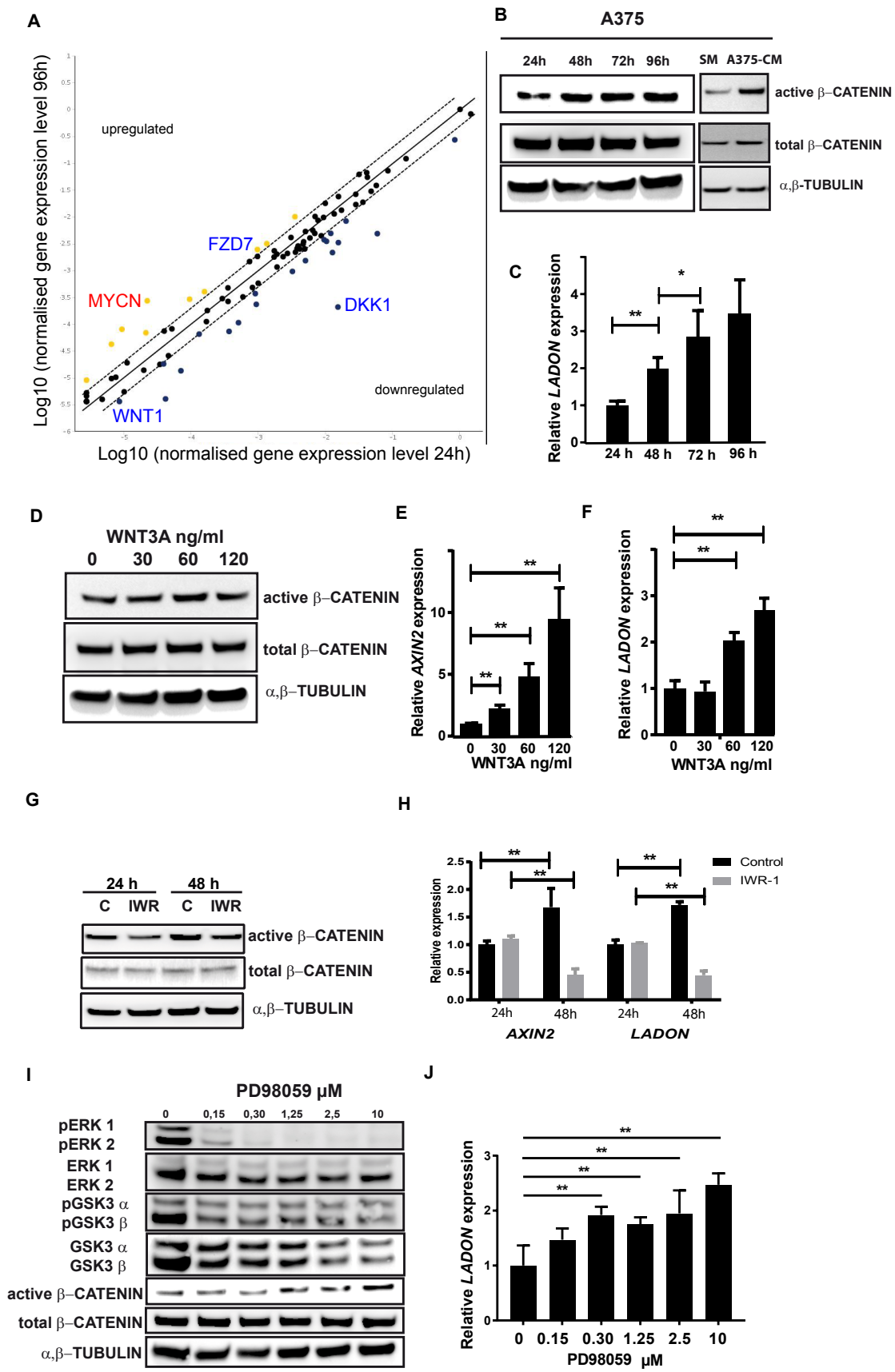
A
Log10 (normalised gene expression level 96h)
Log10 (normalised gene expression level 24h)
upregulated
downregulated
FZD7
MYCN
DKK1
WNT1
B
A375
24h 48h 72h 96h
SM A375-CM
active β–CATENIN
total β–CATENIN
α,β-TUBULIN
C
Relative LADON expression
24 h 48 h 72 h 96 h
D
WNT3A ng/ml
0 30 60 120
active β–CATENIN
total β–CATENIN
α,β–TUBULIN
E
Relative AXIN2 expression
WNT3A ng/ml
F
Relative LADON expression
WNT3A ng/ml
G
24 h 48 h
C IWR C IWR
active β–CATENIN
total β–CATENIN
α,β–TUBULIN
H
Relative expression
Control
IWR-1
24h 48h 24h 48h
AXIN2 LADON
I
PD98059 μM
0 0,15 0,30 1,25 2,5 10
pERK 1
pERK 2
ERK 1
ERK 2
pGSK3 α
pGSK3 β
GSK3 α
GSK3 β
active β–CATENIN
total β–CATENIN
α,β–TUBULIN
J
Relative LADON expression
0 0.15 0.30 1.25 2.5 10
PD98059 μM

Figure 3. *LADON* expression is dependent on WNT/β-catenin signaling.

(A) Scatterplot of the microarray analysis showing how the expression levels of 84 informative genetic markers change in A375 cells cultured for 96h vs 24h. Upregulated genes are in yellow, downregulated genes are in dark blue; black dots represent genes that are not differentially expressed. Only changes in expression levels with a fold change > 2 were taken into consideration (see also Table S3B).
(B) Representative immunoblots for active β-CATENIN, total β-CATENIN and α,β-TUBULIN in A375 cells cultured in standard medium (SM) for up to 96h, or cultured in SM or A375-conditioned medium (A375-CM) for just 24h.
(C) RT-qPCR analysis of *LADON* expression in A375 cells cultured for 24h, 48h, 72h or 96h in SM ($n \geq 3$).
(D) Western blot analysis of lysates from A375 cells treated with increasing doses of WNT3A for 24h. Active β-CATENIN, total β-CATENIN, total α,β-TUBULIN levels are shown.
(E and F) RT-qPCR analysis of *AXIN2* and *LADON* expression in A375 cells treated with increasing doses of WNT3A. *AXIN2* and *LADON* expression levels are normalized to that of endogenous *RPL13*. Values obtained for control conditions (0 ng/ml WNT3A) are normalized to 1.
(G) Western blot analysis of lysates from A375 cells treated with IWR-1-endo (IWR) for 24h or 48h. Active β-CATENIN, total β-CATENIN and α,β-TUBULIN levels are revealed.
(H) RT-qPCR analysis of *AXIN2* and *LADON* expression in A375 cells treated with IWR-1-endo (IWR) for 24h and 48h. *AXIN2* and *LADON* expression levels are normalized to that of endogenous *RPL13*. Values obtained for control conditions (0 ng/ml IWR at 24h) are normalized to 1.
(I) Western blot analysis of lysates from A375 cells treated with increasing doses of PD98059 for 24h. pERK1/2, ERK 1/2, pGSK3α/β, GSK3α/β, active β-CATENIN, total β-CATENIN, total α,β-TUBULIN levels are revealed.
(J) RT-qPCR analysis of *LADON* expression in A375 cells treated for 24h with increasing doses of PD98059. *LADON* expression levels were normalized to those of endogenous *RPL13* expression. Values obtained for control conditions (0 ng/ml PD98059) are normalized to 1.
Histograms display mean values from a minimum of three independent replicates. Error bars indicate SD. The p-values were calculated by Student's t test from three independent experiments. *p< 0,05, **p< 0.01.

Figure 4

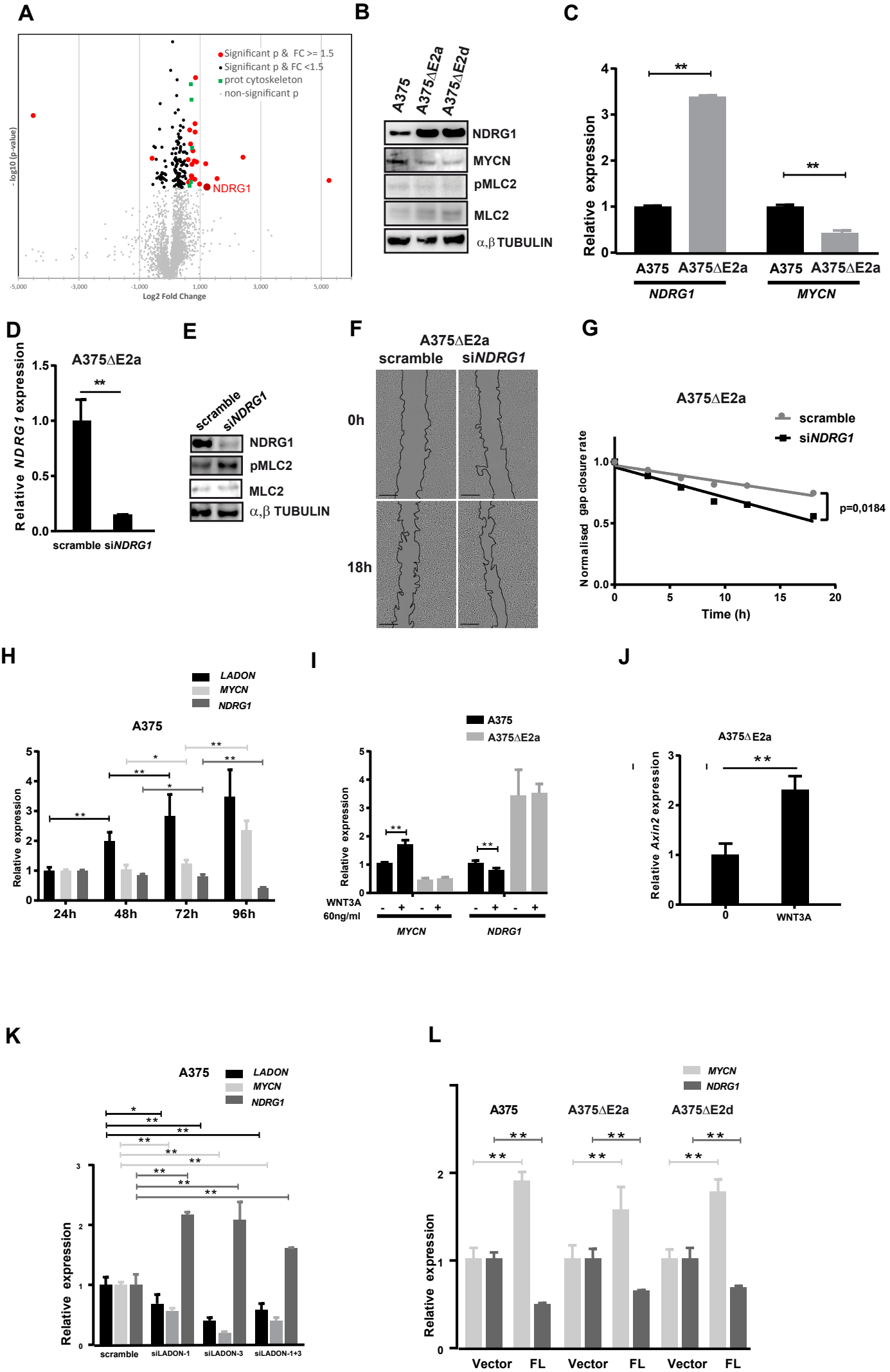
A
Significant p & FC >= 1.5
Significant p & FC <1.5
prot cytoskeleton
non-significant p
NDRG1
- log10 (p-value)
Log2 Fold Change
B
A375
A375ΔE2a
A375ΔE2d
NDRG1
MYCN
pMLC2
MLC2
α,β TUBULIN
C
Relative expression
A375
A375ΔE2a
NDRG1
MYCN
D
A375ΔE2a
Relative NDRG1 expression
scramble
siNDRG1
E
scramble
siNDRG1
NDRG1
pMLC2
MLC2
α,β TUBULIN
F
A375ΔE2a
scramble
siNDRG1
0h
18h
G
A375ΔE2a
scramble
siNDRG1
Normalised gap closure rate
p=0,0184
Time (h)
H
LADON
MYCN
NDRG1
A375
Relative expression
24h
48h
72h
96h
I
A375
A375ΔE2a
Relative expression
WNT3A
60ng/ml
MYCN
NDRG1
J
A375ΔE2a
Relative Axin2 expression
0
WNT3A
K
A375
LADON
MYCN
NDRG1
Relative expression
scramble
siLADON-1
siLADON-3
siLADON-1+3
L
MYCN
NDRG1
A375
A375ΔE2a
A375ΔE2d
Relative expression
Vector
FL

Figure 4. ***LADON* promotes A375 motility by inhibiting the expression of the metastasis suppressor NDRG1**

(A) Volcano plot representation of proteomics analysis in A375 vs A375ΔE2 cells. Grey dots: non-significant p-value. Black dots, significant p-value and fold change < 1,5. Red dots: significant p-value and fold change > 1,5. See also Table 1.

(B) Western blot analysis of lysates from A375 and A375ΔE2a, d cells. NDRG1, MYCN, pMLC2, MCL2 and α β-TUBULIN.

(C) RT-qPCR analysis of *NDRG1* and *MYCN* expression in A375 cells and A375ΔE2a cells. Expression levels are normalized to that of endogenous RPL13. Values obtained for A375 cells are normalized to 1.

(D) RT-qPCR analysis of NDRG1 expression in A375ΔE2a cells treated with scramble siRNA or siNDRG1. Values obtained for A375ΔE2 cells treated with scramble siRNA are normalized to 1.

(E) Western blot analysis of lysates from A375ΔE2a cells treated with scramble siRNA or siNDRG1. NDRG1, pMLC2, MCL2 and α β-TUBULIN levels are revealed.

(F) Representative images, acquired at t=0 and t=18h, of scratch-wound healing assays performed using A375ΔE2a cells treated with scramble siRNA or siNDRG1.

(G) Quantification of the migration rates of the A375ΔE2a cells shown in (F). The p-values are calculated via a two-way ANOVA test.

(H) RT-qPCR analysis of the expression dynamics of *LADON*, *MYCN* and *NDRG1* in A375 cells over a 96h culture. Values obtained at t=24h are normalized to 1.

(I) RT-qPCR analysis of *NDRG1* and *MYCN* expression in A375 and A375ΔE2a cells treated with vehicle or 60 ng/ml WNT3A. Values obtained for control A375 samples are normalized to 1.

(J) RT-qPCR analysis of *AXIN2* expression in A375ΔE2a cells treated with vehicle or 60 ng/ml WNT3A, showing that the treatment does activate WNT/β-CATENIN signaling in these cells. Values obtained with vehicle are normalized to 1.

(K) RT-qPCR analysis of *LADON*, *MYCN* and *NDRG1* expression in A375 cells treated with scramble siRNA, siLADON-1, siLADON-3, or siLADON-1 and -3. Values obtained with the scramble siRNA are normalized to 1.

(L) RT-qPCR analysis of *MYCN* and *NDRG1* expression in A375, A375ΔE2a and A375ΔE2d cells transfected with GFP alone (vector) or together with *LADON* full length (FL). Values obtained for cells treated with vector are normalized to 1.

Histograms display mean values from a minimum of three independent replicates. Error Bars indicate SD. The p-values were calculated by Student's t test from three independent experiments. *p< 0,05, **p< 0.01.

Table 1A.

Max fold change	Description	Filamentous Actin	Stress Fiber	Lamellipodium	Highest mean condition	Accession	Anova (p)
1,606767329	PDZ and LIM domain protein 4 (PDLIM4)	X	X	X	Mutant	P50479	0,0016411
1,637021061	1-phosphatidylinositol 4,5-bisphosphate phosphodiesterase gamma-1 (PLCG1)			X	Mutant	P19174	0,00271601
1,664529632	Dynactin subunit 4 (DCTN4)		X		Mutant	Q9UJW0	0,01351308
1,618822307	Fermitin family homolog 2 (FERMT2)	X	X	X	Mutant	Q96AC1	0,0415036
1,580463985	Nck-associated protein 1 (NCKAP1)	X		X	Mutant	Q9Y2A7	0,047219

Table 1B.

Max fold change	Description	Fonction	Highest mean condition	Accession	Anova (p)
2,274639991	Protein FAM107B (FAM107B)	tumor suppressor	Mutant	Q9H098	0,02268322
38,17912767	Prostatic acid phosphatase (ACPP)	tumor suppressor, regulated by p65	Mutant	P15309	0,03938661
22,78074964	Serine/threonine-protein phosphatase 4 regulatory subunit 2 (PPP4R2)	overexpression in cancer promotes cell growth and invasion	WT	Q9NY27	0,00461911
5,3358974	Transcription factor p65 (RELA)	transcription factor, cell proliferation, apoptosis and oncogenesis	Mutant	Q04206	0,01828842
2,33790023	Protein NDRG1 (NDRG1)	metastasis suppressor	Mutant	Q92597	0,04885314
2,947432444	Gamma-aminobutyric acid receptor-associated protein-like 2 (GABARAPL2)	Ubiquitin-like modifier involved in intra-Golgi traffic	Mutant	P60520	0,03702373

Table 1. Differentially expressed proteins between A375 cells and *LADON* depleted A375ΔE2 cells.

(A) Gene Ontology (GO) term analysis of differentially expressed proteins thus obtained showed a significant enrichment in 5 proteins involved in the composition of filamentous actin.

(B) Proteins with a fold change superior to 2. Proteins were designated significant based on cutoff p value <0.05

Figure 5

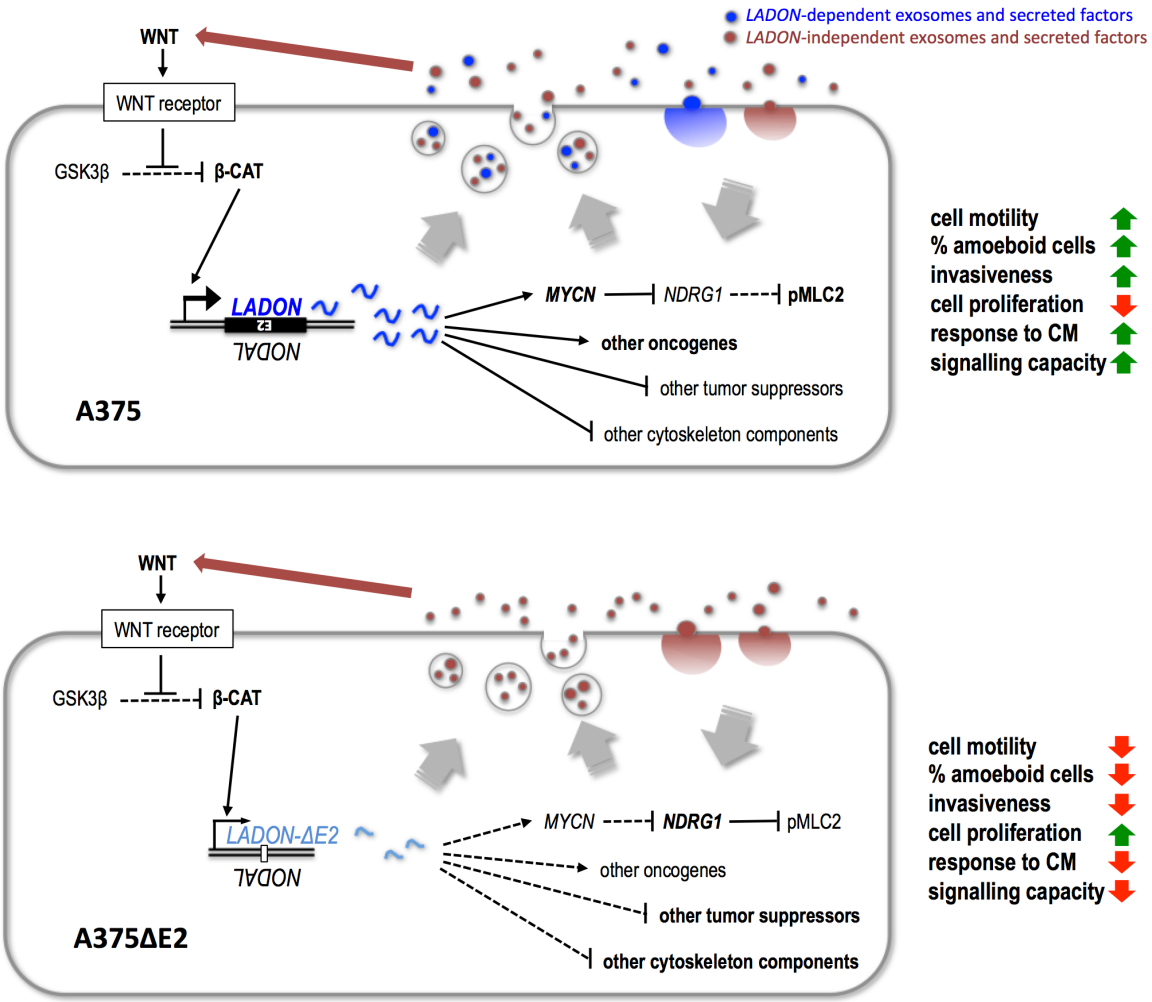
LADON-dependent exosomes and secreted factors
LADON-independent exosomes and secreted factors
WNT
WNT receptor
GSK3β
β-CAT
LADON
E2
NODAL
MYCN
NDRG1
pMLC2
other oncogenes
other tumor suppressors
other cytoskeleton components
A375
cell motility
% amoeboid cells
invasiveness
cell proliferation
response to CM
signalling capacity
WNT
WNT receptor
GSK3β
β-CAT
LADON-ΔE2
NODAL
MYCN
NDRG1
pMLC2
other oncogenes
other tumor suppressors
other cytoskeleton components
A375ΔE2
cell motility
% amoeboid cells
invasiveness
cell proliferation
response to CM
signalling capacity

Figure 5. The comparison of A375 and A375ΔE2 cells supports a role for *LADON* in melanoma metastasis.

In melanoma A375 cells, the *LADON* transcript (in blue) promotes the transition from a proliferative cell identity to a less proliferative and more invasive cell identity. In the course of a 4-day culture, a WNT/β-CATENIN-dependent increase of *LADON* expression promotes the expression of known oncogenes and represses that of tumor or metastasis suppressor, which in turn affect the expression of downstream targets, such as cytoskeleton components. *LADON* notably promotes the expression of the oncogene MYCN, which represses that of the tumor suppressor NDRG1, thus allowing the formation of pMLC2, a cytoskeleton component of migratory cells.

LADON expression also affects the potency of the conditioned medium produced by the cells, presumably via its impact on the exosomes (quantity, content) and the secreted factors they release. *LADON*-dependent exosomes and secreted factors (in blue) promote the progression of exposed melanoma cells towards their more invasive identity. The *LADON* transcript is itself enriched in exosomes.

In A375ΔE2 cells WNT/β-CATENIN signaling does not elicit an increase in the expression of the mutant allele of *LADON-ΔE2*. The expression of its truncated transcript fails to activate or to repress the expression of oncogenes and tumor suppressors as the intact *LADON* transcript does in native A375 cells. One of the consequences is that the expression of NDRG1 is not repressed by MYCN, and the formation of pMLC2 is inhibited. Another is that the conditioned medium of mutant cells is far less effective at promoting the change in phenotype.

The differences found at the molecular level between A375 and A375ΔE2 cells are consistent with their notable differences in cell motility, percentage of amaeboid cells, invasiveness and cell proliferation. Together they support a broad role for *LADON* in the acquisition of a more invasive, less proliferative, melanoma cell identity, a key step in the metastatic process.